Polar N-terminal Residues Conserved in Type 2 Secretion Pseudopilins Determine Subunit Targeting and Membrane Extraction Steps during Fibre Assembly

Javier Santos-Moreno, Alexandra East, Ingrid Guilvout, Nathalie Nadeau, Peter J. Bond, Guy Tran van Nhieu, Olivera Francetic

▶ **To cite this version:**

Javier Santos-Moreno, Alexandra East, Ingrid Guilvout, Nathalie Nadeau, Peter J. Bond, et al.. Polar N-terminal Residues Conserved in Type 2 Secretion Pseudopilins Determine Subunit Targeting and Membrane Extraction Steps during Fibre Assembly. Journal of Molecular Biology, 2017, 429 (11), pp.1746 - 1765. 10.1016/j.jmb.2017.04.005 . pasteur-01602354

HAL Id: pasteur-01602354
https://pasteur.hal.science/pasteur-01602354

Submitted on 2 Oct 2017

HAL is a multi-disciplinary open access archive for the deposit and dissemination of scientific research documents, whether they are published or not. The documents may come from teaching and research institutions in France or abroad, or from public or private research centers.

L'archive ouverte pluridisciplinaire **HAL**, est destinée au dépôt et à la diffusion de documents scientifiques de niveau recherche, publiés ou non, émanant des établissements d'enseignement et de recherche français ou étrangers, des laboratoires publics ou privés.

Polar N-terminal residues conserved in type 2 secretion pseudopilins determine subunit targeting and membrane extraction steps during fibre assembly

Javier Santos-Moreno[1-5#], Alexandra East[6], Ingrid Guilvout[7,8], Nathalie Nadeau[7], Peter J. Bond[9,10], Guy Tran Van Nhieu[2-5] and Olivera Francetic[7,8*]

[1]Université Paris Diderot (Paris 7) Sorbonne Paris Cité
[2]Laboratory of Intercellular Communication and Microbial Infections, CIRB, Collège de France, Paris, France
[3]Institut National de la Santé et de la Recherche Médicale (Inserm) U1050, France
[4]Centre National de la Recherche Scientifique (CNRS), UMR7241, France
[5]MEMOLIFE Laboratory of Excellence and Paris Sciences et Lettres, France
[6]Centre for Molecular Informatics, Department of Chemistry, University of Cambridge, Lensfield Road, Cambridge, CB2 1EW, UK
[7]Laboratory of Macromolecular Systems and Signalling, Institut Pasteur, Department of Microbiology and CNRS ERL6002, 25 rue du Dr Roux, 75724 Paris, Cedex 15, France
[8]Biochemistry of Macromolecular Interactions Unit, Department of Structural Biology and Chemistry, 28 rue du Dr Roux, 75724 Paris, Cedex 15, France
[9] Bioinformatics Institute (A*STAR), 30 Biopolis Str, #07-01 Matrix, Singapore 138671
[10] National University of Singapore, Department of Biological Sciences, 14 Science Drive 4, Singapore 117543

[#]Current address: Department of Fundamental Microbiology, University of Lausanne, Biophore building, CH1015 Lausanne, Switzerland.

[*]Correspondence:
Institut Pasteur, 25 rue du Dr Roux, 75724 Paris CEDEX 15, France
email: ofrancet@pasteur.fr
Tel: 33 1 40 61 36 81
Fax: +33 1 45 68 89 60

Key words: type 4 fibre assembly, membrane proteins, immunofluorescence microscopy, molecular dynamics simulations, N-methylation

Abstract

Bacterial type 2 secretion systems (T2SS), type 4 pili (T4P) and archaeal flagella assemble fibres from initially membrane-embedded pseudopilin and pilin subunits. Fibre subunits are made as precursors with positively charged N-terminal anchors, whose cleavage *via* the prepilin peptidase, essential for pilin membrane extraction and assembly, is followed by N-methylation of the mature (pseudo)pilin N-terminus. The conserved Glu residue at position 5 (E5) of mature (pseudo)pilins is essential for assembly. Unlike T4 pilins, where E5 residue substitutions also abolish N-methylation, the E5A variant of T2SS pseudopilin PulG remains N-methylated, but is affected in interaction with the T2SS component PulM. Here, biochemical and functional analyses showed that the PulM interaction defect only partly accounts for the $PulG^{E5A}$ assembly defect. First, $PulG^{T2A}$ variant, equally defective in PulM interaction, remained partially functional. Furthermore, pseudopilus assembly defect of *pulG(E5A)* mutant was stronger than that of the *pulM* deletion mutant. To understand the dominant effect of E5A mutation, we used molecular dynamics simulations of $PulG^{E5A}$, methylated $PulG^{WT}$ ($MePulG^{WT}$) and $MePulG^{E5A}$ variant in a model membrane. These simulations pointed to a key role for an intra-molecular interaction between the pseudopilin N-terminal amine and E5 to limit polar interactions with membrane phospholipids. N-methylation of the N-terminal amine further limited it interactions with phospholipid head-groups to facilitate pseudopilin membrane escape. By binding to polar residues in the conserved N-terminal region of PulG, we propose that PulM acts as chaperone to promote pseudopilin recruitment and coordinate its membrane extraction with subsequent steps of the fibre assembly process.

Introduction

Prokaryotes build diverse surface appendages and protein transport systems to colonize their niche and acquire nutrients. Some of the most ancient and versatile prokaryotic nanomachines that mediate these functions belong to the type 4 filament (Tff) superfamily [1]. These conserved membrane complexes use the ATP-derived energy to drive assembly of flagella (archaella) and pili in archaea [2; 3; 4] and to build T4P and T2SS pseudopili in bacteria. Illustrating the diversity of Tff functions, T4P, thin bacterial surface fibres, mediate adherence, aggregation, motility, protein transport and DNA uptake [1; 5]. In T2SSs, found in Gram-negative (or diderm) bacteria, short periplasmic pseudopilus fibres promote protein transport from the periplasm across the outer membrane (OM) [6; 7; 8].

Bacterial Tffs are helical polymers of repeating subunits of the major pilin or pseudopilin, which may also contain one or more minor subunits that modulate the fibre assembly and function [1]. These subunits are made as membrane-embedded precursors, with an N-terminal cytoplasmic pre-peptide, followed by a highly conserved transmembrane segment (TMS) and a variable periplasmic globular domain that determines surface features of assembled fibres. The prepilin peptidase, an integral membrane aspartic protease, cleaves the positively charged peptide anchor on the cytoplasmic face of the TMS [9]. Bacterial prepilin peptidases have an additional, methyl-transferase domain that modifies the N-terminus of mature (pseudo)pilins; however the function of this N-methylation remains unclear [10; 11].

In Gram-negative bacteria, Tff assembly systems form large envelope-spanning complexes that have been visualised recently for T4P by cryo-electron tomography [12]. Their most conserved parts are the cytoplasmic hexameric ATPase of the GspE family and the inner membrane (IM) platform protein of the GspF family [13]. Together with GspL and GspM, they

form the assembly platform (AP) [14], which connects *via* the IM protein GspC with the GspD multimer forming the outer membrane secretin channel [15].

In the T2SS of *Klebsiella*, dedicated to secretion of pullulanase (PulA), overproduction of the major pseudopilin PulG leads to assembly of fibres on the cell surface in plate-grown bacteria [16]. A similar phenomenon has been observed for the *Pseudomonas* T2SSs called Xcp [17]. Fibre assembly in overexpression conditions globally correlates with the ability of these systems to promote protein transport under physiological conditions, suggesting a mechanistic link between these two functions [16]. Some interactions of the T2SS major pseudopilin with assembly components have been recently unveiled. The PulG homologue in *Vibrio cholerae*, EpsG, forms a cross-linked heterodimer with EpsL, even in the absence of other Eps components [18]. EpsL is a bitopic IM protein that binds the ATPase EpsE *via* its cytoplasmic domain [19; 20; 21] and has been proposed to couple ATP hydrolysis to major pseudopilin polymerization [18]. Direct interaction of PulL and PulM T2SS homologues in different bacteria leads to their mutual stabilisation [19; 22; 23; 24]. Recent studies using bacterial two-hybrid (BAC2H) and co-purification approaches have shown that PulG interacts individually with PulM and PulF components of the inner membrane assembly platform [25]. Binding of major pilins to PulF, PulL and PulM homologues has also been demonstrated in the T4P assembly system of *Neisseria meningitidis* [26], *Thermus thermophilus* [27] and *Pseudomonas aeruginosa* [28], further supporting the direct role of AP in fibre assembly.

In the *P. aeruginosa* and *N. gonorrhoeae* major T4 pilin subunits, residue E5 is essential for pilus assembly and N-methylation [9; 29; 30]. In contrast, PulG variants with E5A or E5V substitutions are still N-methylated [25; 31], nevertheless they are fully deficient in pseudopilus assembly and protein secretion, suggesting that this mutation affects a key step in the process [31; 32; 33; 34]. Recently we showed that residue E5 of PulG is a key determinant of PulG–PulM interaction in the absence of the other T2SS components [25]. Here, we studied the

role of this interaction and PulM function in the context of the T2SS. Since the defective interaction with PulM could not fully explain the loss of function of PulG^{E5A} variant, we used molecular dynamics (MD) simulations to study PulG interactions with model membranes. The results suggested that both E5 and N-methylation reduce polar interactions of pseudopilin N-terminus with membrane phospholipids, revealing an essential stage of Tff assembly.

Results

PulM requirement for PulA secretion and pseudopilus assembly

Recent studies have identified the AP protein PulM as a strong interacting partner of PulG [25]. PulM is a bitopic IM component of the AP that stabilizes PulL, which provides the membrane anchor to the ATPase PulE [19; 22; 23; 24]. Unlike its homologues from *Vibrio* or *Pseudomonas* T2SSs, previous studies showed that PulM is only partially required for PulA secretion in strains overexpressing *pul* genes [24], although it was essential for assembly of PulG pili [16]. Since in the past the roles of some factors involved in secretion had been overlooked due to overexpression, we reinvestigated the role of PulM in PulA secretion under conditions where *pul* genes were expressed at near-physiological levels, in *Escherichia coli* strain PAP5199 carrying the *pcnB* mutation that reduces the copy number of expression plasmids (Materials and Methods).

At near-physiological expression levels, virtually all PulA was secreted in a strain producing all Pul T2SS components (Fig. 1A, WT lanes 5, 6; Fig. 1C) and secretion was abolished in the negative control strains lacking the PulE ATPase or PulG (Fig. 1A, lanes 1-4; Fig. 1C). A newly constructed mutant strain carrying a complete *pulM* deletion (plasmid pCHAP8496, Table 1 and Materials and Methods) had the same phenotype (Fig. 1A, lanes 7,

8; Fig. 1C), showing that PulM is essential for PulA secretion under physiological conditions. As PulM is involved in PulL stabilization, we asked whether function could be restored by co-expressing an extra copy of *pulL* from a P_{lacZ} promoter in a compatible plasmid (Fig. 1A, lanes 9, 10; Fig. 1C). However, increased PulL levels did not improve PulA secretion, suggesting that PulM might play an additional role. The secretion defect of the Δ*pulM* mutant was complemented with *pulM* or *pulLM* expressed *in trans* (Fig. 1A, lanes 13-16; Fig. 1C).

The Pul T2SS is able to assemble PulG into fibres on the bacterial surface, when the *pul* genes are overexpressed from a moderate copy-number plasmid in bacteria cultured on LB agar media [16]. Here, using the new Δ*pulM* allele, we re-assessed the role of PulM in piliation (Materials and Methods) (Fig. 1B). PulG fibres were assembled in a manner fully dependent on PulE ATPase (Fig. 1B, lanes 1, 2 and 5, 6; Fig. 1D), while no signal was observed in the control lacking PulG (Fig. 1B, lanes 3, 4; Fig. 1D). The absence of PulM led to a severe defect, but did not fully abolish piliation (Fig. 1B, lanes 7, 8; Fig. 1D), confirming our previous observations [7]. In contrast, PulL, which recruits PulE to the AP, was essential for piliation (Fig. 1B, lanes 11, 12). Piliation in the Δ*pulM* strain was restored by complementation with *pulM* (Fig. 1B, lanes 13, 14; Fig. 1D), while overproduction of PulL exacerbated the piliation defects in Δ*pulM* + *pulL* and Δ*pulM* + *pulLpulM* strains (Fig. 1B, compare lanes 7, 8 with 9, 10 and 13, 14 with 15, 16; Fig. 1D), indicating that assembly of surface pili requires the correct ratio between these Pul components. PulM was destabilized in the absence of PulL, and the reverse was also true (Fig. 1B) confirming previous observations [24]. Together, these results show that PulM is essential for PulA secretion under physiological expression conditions and that PulG pilus assembly, although very inefficient, was not fully abolished in the Δ*pulM* mutant.

Effect of pul *gene overexpression on piliation and secretion in the* ΔpulM *mutants*

158 To further characterize the *ΔpulM* mutant, we compared its piliation defect to that of
159 the previously characterized *ΔpulI* strain, which lacks PulI, one of the three minor
160 pseudopilins involved in assembly initiation [35]. As expected, the *ΔpulM* mutant was more
161 deficient in pilus assembly compared to the *ΔpulI* strain (Figs. 2A and B). Analysis of the
162 same strains in liquid culture conditions showed that *pul* gene overexpression did not improve
163 PulA secretion in *ΔpulE*, *ΔpulG* and *ΔpulI* mutants. However, more than 10% of PulA was
164 secreted in the *ΔpulM* mutant (Fig. 2C and 2D), confirming previous findings [24] and
165 suggesting that overproduction of another Pul component might compensate for the absence
166 of PulM.
167 To test whether PulG overproduction allows to overcome this defect, we transformed
168 the *pul* mutant strains used above with plasmid pCHAP8568 (Table 1) carrying *pulG* under
169 the control of the *lacZ* promoter. While increased PulG levels did not overcome the
170 requirement for the PulE ATPase, piliation was improved in *ΔpulI* + *pulG* to an extent
171 comparable to that observed for the positive control (*ΔpulG* + *pulG*) (Fig. 2E and F). In
172 contrast, PulG overproduction led only to a marginal increase of PulG in the sheared fraction
173 of the *ΔpulM* mutant, suggesting that PulM is nearly essential, either for T2SS assembly and
174 integrity or for its activity.
175
176 *Analysis of* pulM *phenotype by immunofluorescence (IF) microscopy*
177
178 To assess in more detail the piliation defect of the *ΔpulM* strain, we analysed samples
179 of plate-grown bacteria using IF microscopy and anti-PulG antibodies (Materials and
180 Methods). PulG fibres were detected in strain producing the complete Pul T2SS (WT) and not
181 in the negative controls lacking the PulE ATPase or PulG (Fig. 3A, Δ*E* and Δ*G*). Consistent
182 with the results of the shearing assay, fewer extracellular fibres were detected in the absence

of PulM (Fig. 3A, Δ*M*) compared to the Δ*pulI* mutant (Fig. 3A, Δ*I*) characterised previously [35]. While WT strain produced on average 0.47 ± 0.09 fibres per bacterium, the *ΔpulI* and *ΔpulM* strains produced on average 4-fold and 52-fold fewer fibres per bacterium, respectively (Fig. 3B). The measurements of the length (Y-axis) of individual fibres (dots) show that, compared to WT strain, the *ΔpulI* and *ΔpulM* strains produced longer fibres on average (Fig. 3B). Plotting the relative frequency distributions of the fibre length in WT and *ΔpulI* and *ΔpulM* mutants further illustrates this tendency (Fig. 3C).

The increased PulG levels led to an increase in fibre numbers and median length to a similar extent in all strains (Fig. 4A, B and D). However, while PulG overproduction restored piliation in *ΔpulG* and *ΔpulI* strains, in the *ΔpulM* mutant strain, the piliation defect remained dramatic with only ~10% of PulG found in the sheared fraction (Fig. 2E).

Differential effect of PulG^{E5A} and PulG^{T2A} on pseudopilus assembly and PulA secretion

We showed recently that E5A substitution in PulG strongly affects PulM binding, raising a possibility that functional defects of PulG^{E5A} could be due to the effect on PulG-PulM interaction [25]. Residue E5 is localized in the highly conserved N-terminal TMS of major and minor pseudopilins [33]. Another highly conserved polar residue in this segment of mature pseudopilins and T4 pilins is Thr at position 2 (T2) (Fig. 5A). Interestingly, T2 and E5 show a degree of co-variation when different pseudopilin sequences are aligned (Fig. 5B). This is linked to the absence of E5 in the GspK family of T2SS pseudopilins and to the conservation of A2 residue in these proteins (Fig. S1). To further characterize this conserved N-terminal region of PulG, we generated the PulG^{T2A} variant and tested its interaction with PulM using the BAC2H approach [36]. Full-length PulM and mature PulG or its variants fused to the C-terminus of T18 and T25 fragments of the catalytic domain of the CyaA adenylyl cyclase

208 from *Bordetella pertussis* were co-produced in an *E. coli Δcya* mutant strain DHT1 [37]. Fusion
209 protein interactions resulted in functional complementation and conversion of ATP into
210 cAMP, monitored using the *lacZ* gene as a reporter.

211 The high β-galactosidase activity of strains co-producing PulM- and PulG- hybrids
212 indicated their strong interaction (Fig. 5C), which was negatively affected by the E5A
213 substitution (Fig. 5C) [25]. Similarly, the T2A substitution in PulG led to reduced *lacZ*
214 expression, showing that T2 is also important for PulM-PulG interaction. All these PulG
215 variants were still able to form homo-dimers (Fig. 5C), which is in agreement with the
216 evidence that residues in the globular head, but not in the N-terminal TMS, drive PulG
217 dimerization [34]. As a control of specificity, we substituted another highly conserved residue of
218 PulG TMS, proline at position 22 (P22), by an alanine. The β-galactosidase activity of strains
219 co-producing PulM- and PulG^{P22A}- chimera did not differ significantly from that of strains
220 producing the wild type PulM- and PulG- hybrids, showing a specific role of conserved
221 residues T2 and E5 in PulG interaction with PulM.

222 We next tested the impact of the T2A substitution on PulG function. A *ΔpulG* strain
223 complemented with the *pulG(T2A)* allele showed a ~50% reduced ability to assemble T2SS
224 pili (Fig. 5D and 5E). Likewise, secretion of PulA was reduced by ~50% for the PulG^{T2A}
225 variant, when all of the *pul* genes were co-expressed at physiological levels (Fig. 5F and 5G),
226 showing a phenotype strikingly different from *pulG(E5A)* mutants.

227 Analysis by IF microscopy showed similar trends. In strain carrying *pulG(T2A)* allele,
228 two-fold fewer fibres were observed relative to *pulG*^{WT}, and the defect was less severe than
229 for *ΔpulM* + *pulG* and *ΔpulG* + *pulG(E5A)* (Fig. 4A). Surprisingly, surface fibres in *ΔpulG* +
230 *pulG(T2A)* strain were shorter on average than those of the positive control *ΔpulG* + *pulG*
231 (Fig. 4A, C and E). Although small, this difference is highly statistically significant and raises

232 the possibility that the T2A mutation might also affect fibre elongation, for example by
233 impairing recruitment of PulG subunits to the AP.
234
235 *PulG interaction with PulM in the context of the Pul T2SS*
236
237 Despite their functional differences, in the BAC2H assay the $PulG^{T2A}$ and $PulG^{E5A}$
238 variants were similarly impaired in interaction with PulM. To test whether PulG and $PulG^{E5A}$
239 interacted with PulM in the context of the complete T2SS, we used a cross-linking approach.
240 *E. coli* PAP7460 bacteria moderately overproducing the Pul T2SSs and different PulG
241 variants were treated with 0.6% formaldehyde (FA), and complexes containing PulM were
242 detected using anti-PulM antibodies (Materials and Methods). In addition to PulM monomers
243 and homo-dimers, we observed a ~38 kDa band that corresponds to a PulG-PulM heterodimer
244 (Fig. 6, G-M), as it was only present in strains producing PulG (Fig. 6). Further supporting its
245 identity as a G-M heterodimer, this band showed shifts in migration dependent on the
246 molecular mass of co-produced PulG and its variants containing a C-terminal hexahistidine
247 tag (Fig. 6, lanes 3, 4) or containing, in addition, the 6-residue long N-terminal pre-peptide (in
248 strain lacking PulO, Fig. 6, lane 2). The levels of PulM-$PulG^{E5A}$-His_6 heterodimer were
249 reduced relative to PulM-PulG-His_6. However, consistent with the PulM-PulG interaction
250 study [25], the E5A substitution in PulG did not fully abolish its interaction with PulM in the
251 context of the T2SS, failing to fully account for its dramatic effect on PulG assembly and
252 function.
253
254 *Molecular dynamics simulations of PulG and its variants in POPE model membrane*
255

Compared to PulG^{WT}, variant PulG^{E5A} is more stable [34] and accumulates in bacteria to higher levels, even in the absence of other T2SS components [25]. We therefore hypothesized that PulG^{E5A} might be blocked in the membrane prior to entry into the assembly pathway. To test this possibility, we used atomistic MD simulations of PulG in model membranes *in silico.* This approach allowed us to study conformations and dynamics of PulG in its native environment and to quantify its atomic contacts with the membrane and solvent. Following cleavage by prepilin peptidase, PulG is N-terminally methylated at the conserved Phe residue (hereafter designated MeF1) [10]. Previous analyses using mass spectrometry showed that most of PulG^{E5A} was methylated whereas ~30% of PulG^{E5A} that co-assembled with PulG^{WT} into mixed pili remained non-methylated [25]. To compare all these forms of PulG, we embedded structural models of a methylated MePulG^{WT}, as well as those of methylated MePulG^{E5A} and non-methylated PulG^{E5A} monomers, into 1-palmitoyl-2-oleoyl-*sn*-glycero-3-phosphoethanolamine (POPE) model membranes, and performed independent triplicate 200-350 ns MD simulations of each.

Initial and representative final snapshots of these simulations (Fig. 7) show that, in the final snapshot, the protein TMS became more deeply buried and its head domain bent towards the lipid membrane surface to varying degrees. The exception was one of the PulG^{E5A} simulations, wherein the bottom of the globular domain nevertheless interacted extensively with the lipid by the end of the simulation. The solvent-accessible surface area (SASA) of residues 60-125, the bulk of the globular domain, decreased on average between ~0.2 and ~3.1 nm^2 over the course of the simulations. Overall the MD simulations did not reveal any statistically significant variations in protein conformation between variants, and SASA suggested that the globular domain does not maintain strong, consistent contacts with POPE. As expected, the E5A variants did not cause severe protein destabilization or membrane perturbation, supporting the notion that the role of E5 is localized to the N-terminus.

Next, we compared the maintenance of the protein secondary structure during each simulation. In all the systems, the N-terminal α-helix, with the exception of the first 4 residues, was almost entirely conserved throughout the simulations, as were the two β-sheets between residues 97-102 and 110-114. Transient disruptions to the α-helix were observed in one PulG^{E5A} simulation (with residues 30-34, or solely residue 34, losing their helical structure) and in one MePulG^{WT} simulation (where the helix disintegrated around either residues 27-30 or again around residue 34). However, helix integrity was fully restored by the end of these simulations. On the other hand, we observed significant differences in the secondary structure of the five N-terminal residues between wild type and E5A variants. In all MePulG^{WT} simulations the first several residues demonstrated a relaxation of helical structure into either turns or coils, as illustrated in Figure 8. In contrast, in the MePulG^{E5A} and PulG^{E5A} systems, the five N-terminal residues maintained their helical structure throughout, except in one Me-PulG^{E5A} simulation, where six N-terminal residues transiently formed a 3-10 helix or turn structure between ~150-200 ns. Together, these results suggested that the residue E5 affects the secondary structure of the PulG N-terminus.

To study this phenomenon more closely, we quantified the proximity of E5 to the N-terminus in all simulations. The distance between the centres-of-mass (COM) of residues 1 and 5 was largely fixed due to the helix on which they are both located. However, significant differences were observed in the minimum distance between the residue 1 methyl group or amide terminus (depending on whether the system contained MeF1 or F1) and any atom of the residue 5 side-chain (Fig. 9A). Notably, in the MePulG^{WT} system the methyl group of MeF1 and the E5 side-chain remained consistently within 3 Å of each other, indicating their electrostatic contact. This was not the case in the simulations of PulG variants carrying the E5A substitution. In the PulG^{E5A} system, the A5 side-chain made no contact with F1 and remained at 6 Å distance, only approaching to within 5 Å in two simulations, and solely in the

first 30 or 70 ns. The MePulG^{E5A} simulations showed more fluctuation, with the atoms approaching to within ~2.5 Å and moving as far as 10 Å apart; however, the side-chains mostly remained ~6 Å apart. Visual analysis shown in Fig. 9B supported these results; E5 and MeF1 remained close in MePulG^{WT}, while in the MePulG^{E5A} system A5 stayed embedded in lipid whereas MeF1 was extensively solvated. Importantly, in MePulG^{WT} the N-terminal amine was engaged in interaction with E5 and did not form polar contacts with POPE phosphate groups, while in PulG^{E5A} it was anchored to three different POPE molecules towards the end of the simulation (Fig. 9B). The MePulG^{E5A} showed an intermediate behaviour, with reduced amine interactions with POPE, perhaps explaining the fluctuating distances to A5 during MD simulations. These data suggest that in MePulG^{WT} E5 promotes intra-molecular interactions with the N-terminal positive charge of MeF1, thus reducing the polar contacts with phospholipid head-groups, and potentially priming the protein for membrane extraction during pseudopilus assembly. In contrast, the N-termini of the mutant variants interacted with membrane phospholipids, anchoring the protein more firmly in the bilayer.

Relative to the mutant systems, the MePulG^{WT} experienced extended periods with no hydrogen bonds to solvent water, and its MeF1 formed 0.6 hydrogen bonds to water, on average. The MeF1 from MePulG^{WT} and MePulG^{E5A} proteins formed on average ~0.9 hydrogen bonds with POPE, relative to the ~1.9 hydrogen bonds formed by F1 from non-methylated PulG^{E5A}. When normalised relative to the number of possible hydrogen bonds from each, this analysis demonstrated that F1 engaged in hydrogen bonding to phospholipid 40% more than MeF1. The methylation therefore decreased the number of hydrogen bonds to phospholipid head-groups, which might reduce the energetic cost of transferring the charged N-terminus across the IM.

T2 residue dynamics were also explored. T2 in MePulG^{WT} formed only one hydrogen bond to E5 during a single simulation frame, and only sporadic hydrogen bonds were observed between the T2 hydroxyl oxygen and the MeF1 benzene ring. Instead, T2 formed on average ~1.4 hydrogen bonds with water and ~0.9 hydrogen bonds with surrounding POPE molecules. Likewise, in the MePulG^{E5A} variant, T2 formed on average ~1.3 and ~0.8 hydrogen bonds to water and to POPE respectively, and did not form any bonds with MeF1. Altogether, the simulations suggested that in the wild type, E5 engages in interaction with MeF1, leaving T2 available for interactions with solvent, membrane or other proteins, possibly PulM. The variation of residue 5 did not have a significant effect on T2 dynamics.

Discussion

To elucidate the early steps of pseudopilus assembly, we focused in this study on the interactions of the major pseudopilin PulG with the PulM AP component of the *K. oxytoca* T2SS. The results showed that PulM is fully required for PulA secretion under physiological conditions. On the other hand, overproduction of T2SS components resulted in dramatically reduced (but not fully abolished) PulA secretion and PulG fibre assembly in the *pulM* knockout. This is in agreement with results obtained in *P. aeruginosa* lacking its homologue XcpZ, which also shows low levels of piliation [38]. Quantitative IF microscopy analysis indicated that *pulM* mutants assemble at least 50-fold less pili compared to wild type. This defect is probably underestimated, since only fields containing at least one pilus were taken into account during IF quantification (Materials and Methods). Contrary to our predictions, the fibre length was not reduced but rather increased in Δ*pulM* mutants.

The fact that overproduction of PulG could not restore efficient piliation in *ΔpulM* strains, together with reduced PulL levels is consistent with a requirement of PulM for

assembly of the functional T2SS complex [25]. The recent insights into the *Myxococcus xanthus* T4P machinery from cryo-electron tomography reveal a continuous, envelope-spanning apparatus [12]. Given the structural similarities between T4P and T2SSs, it is likely that the T2S nano-machine is organized in a similar manner, so that PulM, together with PulL, might constitute the lower periplasmic electron-dense ring in the periphery of the complex. In *M. xanthus*, this ring is absent in bacteria lacking PilO, which is a probable PulM equivalent sharing the same topology [12]. Studies of T2SS GFP chimera using live fluorescence microscopy support the localization of the *V. cholerae* PulM homologue EpsM in fluorescent foci dependent on the GspD, GspC and GspL homologues [39]. Since PulD-mCherry chimera form similar fluorescent foci in the absence of other Pul factors, the secretin assembly probably initiates the assembly of the T2SS complex [40]. These and other studies suggest that PulM might serve as a link bringing together the pseudopilin/PulF complex and the PulD/C/L complex through its interactions with PulG/PulH on one hand and PulL on the other [19; 22; 23; 24; 25]. Therefore, the observed critical role of PulM in fibre assembly could be due to its requirement for building a functional T2SS machine and its role in PulL stabilization, documented in several T2SSs [19; 22; 23; 24]. The rare PulG fibres that form in *ΔpulM* mutants under overexpression conditions might stem from the few T2SS complexes that assemble through a low-affinity interaction of PulG with PulL [25]. The accumulation of unassembled PulG in the IM would drive elongation of pili within these rare T2SS complexes, thereby accounting for the higher median length of fibres in *ΔpulM* mutants. A similar effect was observed previously for the mutants lacking minor pseudopilins of the tip complex, including PulI, used here as a control [35].

In addition to the PulM role in PulL stabilization, its interaction with PulG in the absence of other Pul factors [25] suggested an additional, direct role in pseudopilus assembly. Here, using chemical cross-linking, we showed that PulM and PulG also interact in the

380 presence of other T2SS components, and that the E5A substitution reduced interaction with
381 PulM. Both PulG and PulM are integral membrane proteins that share the N-in C-out
382 topology. In addition to the PulG residue E5, we show here that residue T2 in this region is
383 equally required for PulM interaction in the BAC2H assay, possibly accounting for residual
384 PulM binding of the PulG^{E5A} variant. This is also supported by MD simulation results, where
385 residue T2 remained sterically available for inter-molecular interactions in all variants. The
386 conformation of MePulG^{WT} is compatible with PulM binding *via* T2 residue, which would
387 explain the effects of PulG T2A substitution on PulM interaction and its impact on the fibre
388 length. Furthermore, given that in MD simulations residue E5 of mature MePulG^{WT} is
389 engaged in interactions with the N-terminal amine, T2 might be an important determinant of
390 this interaction during the membrane extraction step of PulG assembly. Since T2 formed
391 hydrogen bonds with the surrounding solvent and membrane in all simulations, PulM binding
392 might shield T2 and reduce these contacts to facilitate PulG membrane extraction, or its
393 transfer to another binding partner. The high conservation of T2 and E5 among T2SS
394 pseudopilins and T4 pilins (Fig. 5A) further shows the importance of PulG-PulM interface,
395 whose disruption, at least on the PulG side, correlates with severe functional defects. Testing
396 this model requires mutagenesis studies of the PulM cytoplasmic tail and/or TMS. Although
397 no structural information on this part of PulM and its homologues is available, the predicted
398 topology of these regions makes them obvious candidates for PulG binding.
399 Although the interaction with PulM was affected to a similar extent for PulG^{E5A} and
400 PulG^{T2A} variants in the BAC2H assay, the functional impact of the two substitutions was very
401 different. Compared to the E5A substitution that fully abolished function, the T2A
402 substitution resulted in a partial defect in both fibre assembly and protein secretion (Fig. 5).
403 The weaker PulM - PulG interaction reduced by half the number of assembled pili, which
404 might directly reflect the number of assembled T2SS complexes. In addition, the pseudopili

405 composed of PulG^{T2A} variant showed lower median length compared to wild type. This might
406 reflect reduced fibre stability, in agreement with recent structural analysis of meningococcal
407 T4P that have implicated residue T2 in inter-protomer interactions, involving residue E5 of
408 the protomer below [41]. However, the defective PulA secretion in the presence of PulG^{T2A}
409 supports an early role of T2 in PulG assembly, consistent with previous studies showing that
410 PulG pilus stability is not required for secretion [33; 34]. In this model, PulM binding might
411 facilitate PulG recruitment to the machinery, e.g. by targeting PulG subunits to the active site
412 of the AP. In addition, PulM might act as a chaperone, favouring the PulG conformation
413 compatible with assembly. In *V. cholerae*, a cross-linking study showed direct interaction
414 between the major pseudopilin EpsG and the PulL homologue EpsL [18], and our recent study
415 indicates weak interactions between PulL and PulG [25]. While the absence of prepilin
416 peptidase in *V. cholerae* prevents the EpsG-EpsL cross-linking, in our studies the presence of
417 the prepeptide seems to enhance PulG-PulM interaction, as suggested by the similar levels of
418 heterodimers in the strain lacking PulO, which contained lower levels of PulG monomer (Fig.
419 6, anti-G, lane 2). The preferential binding of precursor and mature forms of major
420 pseudopilin to different partners in the AP - L or M - might reflect different conformations
421 that represent intermediates in the assembly pathway.

422 To gain insight into these PulG conformations in wild type and E5A mutant variants
423 we turned to MD simulations. Unexpectedly, this approach highlighted a role of another
424 interacting partner of PulG - the plasma membrane, which poses a major obstacle to assembly
425 of type 4 filaments in bacteria. By revealing the striking conformational difference between
426 the N-termini of MePulG^{WT} compared to MePulG^{E5A} and PulG^{E5A} variants in the membrane,
427 the results of MD simulations provide a plausible explanation for the phenotypes of
428 *pulG(E5A)* mutants. Contrary to the PulG^{E5A} whose N-terminal amine is firmly anchored in
429 the membrane through polar contacts with up to three different phospholipids, in MePulG^{WT}

residue E5 neutralized the N-terminal membrane anchor. The T4P assembly models proposed by Craig *et al*. [42] and Melville and Craig [5] emphasise the importance of charge neutralisation during fibre assembly. While these models consider the inter-protomer charge neutralisation, the results of MD simulations and (Me)PulG^{E5A} membrane accumulation strongly support the role of intra-molecular neutralisation of the N-terminal amine *via* a loop formation with E5. The intra-molecular contacts between F1 and E5 residues have also been observed in the crystal structure of T4 pilins of the *P. aeruginosa* PAK strain PilA (Protein database (PDB) entry code: 1OQW) and in *N. gonorrhoeae* pilin PilE (PDB: 2HI2) [42; 43]. A similar loop structure is suggested by the MD analyses of the *P. aeruginosa* major T4P subunit PilA [44]. Interestingly, in that study the loop is observed in initial stages of MD simulation, whereas towards the end, when PilA is fully embedded in the membrane, the N-terminal amine interacts with the phospholipid head-groups. The difference compared to our study is that PilA was not modelled with a methyl group, which might have led to ceasing of the intra-molecular F1-E5 interaction by the end of the simulation. Following the positive inside rule [45], the positively charged residues of IM proteins are anchored to the cytoplasmic face of the IM through interactions with negatively charged phosphate groups of membrane phospholipids. Besides, since the MD simulation conditions do not take into account the proton gradient, the membrane anchoring of MePulG^{WT} and (Me)PulG^{E5A} might be even stronger *in vivo* and might represent a rate-limiting step during pseudopilus assembly. Strong membrane association and stable N-terminal helix conformation could explain the decreased turnover rate of the PulG^{E5A} compared to PulG^{WT} as measured previously [34] and its relative accumulation in *E. coli* [25].

The MD simulation results suggest that N-methylation might further reduce polar contacts of pilins with the solvent, contributing to their extraction from the membrane. Our observations using this approach also provide a clue for the link between E5 and N-

455 methylation, observed previously. While the E5K or E5V substitutions in the major subunit of
456 *P. aeruginosa* T4P PilA abolish N-methylation [9; 46], the E5A substitution in PulG only
457 reduces the methylation efficiency by around 30% [25]. Enhanced N-terminal amine contacts
458 with phospholipid head-groups in these variants might block or reduce the access of N-methyl
459 transferase domain of prepilin peptidase to its amine substrate. The different effects of E5
460 residue substitutions on T4 pilins and T2SS pseudopilins might be linked to the differences
461 between their AP components such as PulM, a hypothesis that requires further investigation.
462 Among Tff systems, archaeal pili and flagella do not have the conserved residue E5 [47],
463 and archaeal prepilin peptidases do not have a methyl-transferase domain and activity. One
464 possible explanation for these differences might lie in the different composition of archaeal
465 membranes, formed by tetraether lipids that are structurally and functionally different from
466 bacterial phospholipids [48]. Rare exceptions to this rule include *Aeropyrum pernix* and
467 *Archaeoglobus fulgidus,* where flagellins do have a conserved E5 residue, and whose
468 presence correlates with the documented presence of phospholipids in their membranes [49; 50].
469 However, in most archaea the rules of membrane anchoring for proteins might be very
470 different compared to bacteria. The conserved E5 and N-methylation might represent a
471 bacterial solution to the problem of membrane escape for proteins anchored in the
472 phospholipid membrane. The remarkable efficiency of this strategy and the dramatic effect of
473 E5A mutation provide another example of the importance and the strength of weak bonds in
474 biological systems.
475
476 Overall, the results of this study are compatible with a dual role of PulM binding to
477 PulG. During initial steps of T2SS assembly, PulM might bind the PulG precursor to favour
478 recruitment of pseudopilin-PulF subcomplex to the secretin/AP complex [25]. During fibre
479 elongation, PulM might facilitate PulG targeting to the active site of the T2SS and/or its

480 extraction from the membrane, by favouring a conformation that minimises membrane
481 contacts. These roles for PulM are based on its ability to bind PulG and PulH on one hand and
482 PulL on the other, probably in a dynamic fashion, as shown for its homologues in T2SSs [51]
483 and T4P [52]. Eventually, PulG recruited from the IM pool would reach the assembly focus
484 defined by PulF and the PulE ATPase poised for membrane extraction and incorporation into
485 the pseudopilus. Future studies are needed to reveal the nature of these conformational
486 changes and the precise molecular function of PulM in coordinating PulG membrane
487 extraction with its incorporation into the growing fibre.
488
489 **Materials and Methods**
490
491 *Bacterial strains and culture*
492
493 The *E. coli* DH5α F' *lacI*^{Q} strain was used for cloning purposes. Strain PAP7460
494 [Δ*(lac-argF)U169 araD139 relA1 rpsL150* Δ*malE444 malG501 [F' (lacI*^{Q} Δ*lacZM15 pro+*
495 *Tn10)] (Tc*^{R}*)* [24] was used for *pul* gene expression and strain PAP5299 [*araD139 Δ(argF-*
496 *lac)U169 rpsL150 relA1 flb5301 deoC1ptsF25 thi pcnB::Tn10* (F' *lacI*^{Q})] [33] was employed
497 for secretion assays. Bacteria were grown at 30 ºC in LB medium (10 g L^{-1} bacto tryptone; 5 g
498 L^{-1} yeast extract; 10 g L^{-1} NaCl; pH 7.0) containing antibiotics as required: ampicillin, 100 μg
499 ml^{-1}; chloramphenicol, 25 μg ml^{-1}; kanamycin, 20 μg ml^{-1}. Expression of *pul* genes cloned
500 under the control of the *lac* promoter was induced with 1 mM isopropyl-β-D-thiogalactoside
501 (IPTG). Expression of *pul* genes was induced with 0.4% maltose in LB medium buffered with
502 1/10 volume of M63B1 salt solution (modified from [53]: 13.6 g L^{-1} KH_2PO_4; 2 g L^{-1}
503 $(NH_4)_2SO_4$; 0.2 g L^{-1} $MgSO_4 \cdot 7H_2O$; 0.5 mg L^{-1} $FeSO_4 \cdot 7H_2O$; 1 mg L^{-1} vitamin B1; pH 7.0).
504

505 *Recombinant DNA and plasmid construction*

506 The list of plasmids used in this study is shown in Table 1.

507 **Table 1.** Plasmids used in this study.

508

Name	Ori / Resistance[a]	Relevant characteristics	Reference
pCHAP8185	ColE1 / Ap^R	*pulA*$_{sol}$ all *pul* genes	[35]
pCHAP8184	ColE1 / Ap^R	*pulA*$_{sol}$ all *pul* genes *ΔpulG*	[33]
pCHAP8400	ColE1 / Ap^R	All *pul* genes *ΔpulG ΔpulNO*	This study
pCHAP8200	ColE1 / Ap^R	*pulA*$_{sol}$ all *pul* genes *ΔpulE*	This study
pCHAP8218	ColE1 / Ap^R	*pulA*$_{sol}$ all *pul* genes *ΔpulI*	[35]
pCHAP1217	ColE1 / Ap^R	All *pul* genes *ΔpulL*	[24]
pCHAP8496	ColE1 / Ap^R	*pulA*$_{sol}$ all *pul* genes *ΔpulM*	This study
pCHAP8251	ColE1 / Ap^R	*pulA*$_{sol}$ all *pul* genes *ΔpulL*	This study
pCHAP8811	ColE1 / Ap^R	*pulM*	This study
pCHAP576	ColE1 / Kan^R	*pulO*	[54]
pCHAP8258	p15A / Cm^R	*pulL*	This study
pCHAP1353	p15A / Cm^R	*pulM*	[24]
pCHAP8843	p15A / Cm^R	*pulL-pulM*	This study
pCHAP1362	p15A / Cm^R	*pulG-his*$_6$	[55]
pCHAP7785	p15A / Cm^R	*pulG*^{E5A}*-his*$_6$	This study
pCHAP8658	p15A / Cm^R	*pulG*	[34]
pCHAP8732	p15A / Cm^R	*pulG*^{T2A}	This study
pCHAP8663	p15A / Cm^R	*pulG*^{E5A}	[34]
pCHAP8875	ColE1 / Ap^R	*pulA*$_{sol}$ all *pul* genes *ΔpulG ΔpulM*	This study
pCHAP8377	ColE1 / Ap^R	*pulKLMNO*	This study
pCHAP8395	ColE1 / Ap^R	*pulKLM*	This study
pSU19	p15A / Cm^R	Empty vector	[56]
pBGS18	ColE1 / Km^R	Empty vector	[57]
pUT18c	ColE1 / Ap^R	p*lacZ*-T18	[36]
pKT25	p15A / Km^R	p*lacZ*-T25	[36]
pCHAP8154	ColE1/Ap^R	pUT18c *pulM*	[25]
pCHAP8155	p15A/Km^R	pKT25 *pulM*	[25]
pCHAP7330	ColE1/Ap^R	pUT18c *pulG*	[34]
pCHAP7332	p15A/Km^R	pKT25 *pulG*	[34]
pCHAP8670	ColE1/Ap^R	pUT18c *pulG (E5A)*	[34]
pCHAP8420	p15A/Km^R	pKT25 *pulG (E5A)*	[34]
pCHAP8733	ColE1/Ap^R	pUT18c *pulG (T2A)*	This study
pCHAP8734	p15A/Km^R	pKT25 *pulG (T2A)*	This study
pCHAP8429	ColE1/Ap^R	pUT18c *pulG (P22A)*	This study
pCHAP8482	p15A/Km^R	pKT25 *pulG (P22A)*	This study

509 **a.** Ap, ampicillin; Cm, chloramphenicol; Km, kanamycin.

510 Plasmid pCHAP8200 was generated by replacing the 7430-bp EcoRI-Bsu36I fragment

511 of plasmid pCHAP8185 with the corresponding fragment of plasmid pCHAP1230 carrying

512 the *ΔpulE* allele [24]. Plasmid pCHAP8251 was generated by replacing the EcoRI-HindIII
513 fragment of plasmid pCHAP8185 with the corresponding fragment from pCHAP1217
514 plasmid carrying the nonpolar deletion of the *pulL* gene. Plasmid pCHAP8496 carrying a
515 complete in-frame deletion of *pulM* was generated as follows. Random insertions of the GPS5
516 (Km^R) cassette in the *pulM* gene were generated *in vitro* using the GPS®-LS kit (New England
517 Biolabs). Two insertions of the GPS5 cassette, each marked with a single PmeI site mapping
518 in positions 20 and 120 of *pulM* ORF, were combined in plasmid pCHAP1353 to give
519 pCHAP8370. The *pulM::kan* allele was introduced into pUC18 derivative containing the
520 *pulM* gene, pCHAP8510, to give pCHAP8512. This plasmid was digested with PmeI to create
521 an in-frame deletion of *pulM*, giving pCHAP8513. The DraIII-NsiI fragment containing the
522 *ΔpulM* allele was ligated to the DraIII-NsiI fragment of pCHAP8377 containing the distal half
523 of the *pul* operon, which was obtained by self ligating the AleI fragment of pCHAP231. This
524 yielded plasmid pCHAP8516. In the final step, the NotI-EcoRI A fragment of pCHAP8516
525 was ligated with the large EcoRI-NotI fragment of plasmid pCHAP8185 to give pCHAP8496.
526 Plasmid pCHAP8811 was constructed by sub-cloning the EcoRI-HindIII insert containing the
527 *pulM* gene from plasmid pCHAP1353 into pUC18 vector digested with EcoRI and HindIII.
528 Plasmid pCHAP8732 carrying *pulG(T2A)* allele was generated by Quick-change mutagenesis
529 using primers pulGT2A-5 and pulGT2A-3 (Table S1). Primers PulG T2A-Kpn and PulG Eco-
530 3 were used to amplify the *pulG(T2A)* allele from plasmid pCHAP8732 in KpnI and EcoRI
531 digested BAC2H plasmids pUT18c and pKT25, to yield pCHAP8733 (pUT18c-$pulG^{T2A}$) and
532 pCHAP8734 (pKT25-$pulG^{T2A}$). Plasmid pCHAP8258 was made by cloning the *pulL* gene
533 PCR-amplified with primers PulL-Eco 5 and PulL-Hind 3 in the EcoRI and HindIII sites of
534 pSU18. Plasmid pCHAP8843 was generated by cloning the PCR amplified pCHAP8185
535 fragment containing the *pulL* and *pulM* genes in pSU18 EcoRI and HindIII sites amplified by
536 PCR using PulL-Eco 5 and PulM 3 oligonucleotide primers. All PCR reactions were

performed using the high-fidelity Pwo polymerase (Roche). Plasmid pCHAP8732 was derived from pCHAP8658 by the Quick-change method of site-directed mutagenesis with primers PulG T2A-5 and PulG T2A-3 (Table S1). Plasmid pCHAP8875 was constructed by ligating the pCHAP8184 NotI-HindIII B fragment with the pCHAP8496 NotI-HindIII fragment A. Plasmid pCHAP8400 was made in several steps. First, plasmid pCHAP8377 was constructed by ligating the AleI fragment of pCHAP231 containing the distal half of the *pul* operon. The EcoNI fragment of pCHAP8377 containing *pulN* and *pulO* genes was deleted to give pCHAP8395. The EcoRI-NotI fragments from pCHAP8395 and pCHAP8184 were then combined to reconstitute the *pul* operons with deletions of *pulG*, *pulN* and *pulO*.

All plasmid constructs were verified by sequencing (GATC). The list of oligonucleotides is provided in Table S1.

In vivo *cross-linking* and PulM-PulG interaction analysis.

For the formaldehyde cross-linking, 40 OD_{600} of bacterial cultures were centrifuged (3500 x g, 5 minutes, room temperature). Bacterial pellets were washed with 10 ml PBS and resuspended in PBS at 8 OD_{600} ml^{-1}. Following the cross-linking with 0.6% formaldehyde (Sigma-Aldrich) for 20 minutes at 30°C with vigorous shaking, the bacteria were pelleted for 2 minutes at ~12000 x g and resuspended in 5 ml of 50 mM Tris-HCl (pH 8.0) for 10 minutes at room temperature. The quenched reactions were centrifuged at 8000 x g for 5 minutes and the pellets were resuspended in 2 ml of cold TBS (20 mM Tris-HCl, 150 mM NaCl, pH 7.4) containing cOmplete^{TM} ULTRA EDTA-free (Roche) protease inhibitor cocktail (concentration as indicated by the supplier). The cells incubated on ice for 10 minutes in the presence of 0.2 mg ml^{-1} lysozyme and 0.02 mg ml^{-1} DNase I, followed by sonication at 4°C using the Vibra-Cell Ultrasonic Processor 75186 (Sonics & Materials) at 30% amplitude with

562 1 sec ON / 1 sec OFF cycles for a total sonication time of 10 seconds. The total cell extracts
563 were analysed by SDS-PAGE and immunodetection as described below.
564
565 *Piliation and secretion assays*
566
567 Functional assays to test piliation and secretion were performed as described in [34]. For
568 the shearing assay, bacteria were grown overnight in LB agar plates and expression of *pul*
569 genes was induced by maltose (and IPTG, when required). Bacteria were scraped off the
570 plates and resuspended in LB at 1 OD_{600} ml^{-1}, and 1 ml of the suspensions was vortexed for 1
571 minute to detach surface pili. Upon centrifugation of the samples at ~12000 x g for 5 minutes
572 at 4°C, the pelleted bacteria were resuspended in SDS sample buffer, and the supernatants
573 containing the sheared pili were submitted to TCA (trichloroacetic acid) precipitation. Briefly,
574 the supernatants were centrifuged at ~12000 x g for another 10 minutes at 4°C to remove any
575 remaining bacteria, and pili were precipitated in 10% trichloroacetic acid for 30 minutes on
576 ice. The precipitates were pelleted by centrifugation at ~12000 x g for 30 minutes at 4°C,
577 washed twice with cold (-20°C) acetone, air-dried and resuspended in SDS sample buffer.
578 Equal amounts of cell and sheared fractions were analysed using SDS-PAGE and PulG
579 immunodetection. For the secretion assay, bacteria producing a non-acylated, soluble variant
580 of PulA were grown in LB medium buffered with 0.1 volume of M63 salts, supplemented
581 with 1mM IPTG and 0.2% maltose for the induction of *pul* genes. After normalization of
582 cultures to 2 OD_{600} ml^{-1}, 1 ml was centrifuged at ~12000 x g for 5 minutes at 4°C. The
583 pelleted cells were resuspended in SDS sample buffer. The supernatants were centrifuged
584 again under the same conditions, and a sample was taken from the topmost part of the tube
585 and mixed with 2 x SDS sample buffer. The same OD equivalent amounts of cell and
586 supernatant fractions were analysed by SDS-PAGE and immunodetection of PulA.

587

588 *SDS-PAGE and immunodetection*

589

590 Protein separation was performed by SDS-PAGE in Tris-tricine gels [58] containing
591 10% acrylamide, using Appelex or BioRad vertical gel electrophoresis systems. Proteins were
592 electro-transferred onto Amersham Hybond ECL nitrocellulose membranes (GE Healthcare)
593 using the semi-dry method with a buffer containing 5.8 g L^{-1} Tris base, 2.9 g L^{-1} glycine, 20%
594 ethanol, 0.026% SDS. Membranes were blocked with 5% skim milk in TBST (10mM Tris-
595 HCl, 15mM NaCl, 0.05% Tween20, pH 7.5-7.6), probed for 1 h with specific antiserum
596 (1:2000 anti-PulG, 1:2000 anti-PulA, 1:1000 anti-PulL, 1:500 anti-PulM, 1:2000 anti-LamB,
597 1:10000 anti-RbsB), washed several times with TBST, incubated with secondary antibody
598 (1:20000 or 1:40000 anti-rabbit, horseradish peroxidase-coupled) for 1 h, and washed
599 extensively with TBST. Membranes were developed by enhanced chemiluminescence using
600 Pierce ECL 2 (Thermo Scientific), Western Lightning Plus ECL (PerkinElmer) or
601 SuperSignal West Femto (Thermo Scientific), and the signal was recorded using Typhoon
602 FLA 9000 imager (GE Healthcare) or LAS 4000 imager (Fujifilm). ImageJ software [59] was
603 used for densitometric analysis of bands.

604

605 *Bacterial two-hybrid assay*

606

607 Competent cells of strain DHT1 [37] were co-transformed with pUT18C and pKT25
608 derivatives and bacteria were grown for 48 h at 30°C on LB plates containing Ap and Km. Six
609 colonies were picked at random and inoculated into 5 ml cultures in LB containing Km and
610 Ap, grown overnight and inoculated the next day into fresh medium containing 1 mM IPTG.
611 Bacteria were cultured to mid-log phase and β-galactosidase activity was measured as

612 described [60]. At least 2 independent experiments were performed with several randomly
613 picked transformants. Bar graphs represent mean values and error bars indicate standard
614 deviation. The non-parametric Kruskal-Wallis followed by Dunn's multiple comparison tests
615 were used in statistical analysis using the Graphpad Prism 6 software.
616
617 *Immunofluorescence microscopy*
618
619 IF labelling of pili was performed as described previously [34]. Bacteria grown for 16
620 hours at 30°C on LB agar supplemented with 0.4% maltose were carefully resuspended in
621 PBS at 1 OD_{600} ml^{-1} and immobilized on coverslips coated with poly-L-lysine. After 30
622 minutes of fixation using 3.7% formaldehyde at room temperature, reactions were quenched
623 with 1M Tris-HCl pH 8.0 and samples were blocked with 1% bovine serum albumin (BSA) in
624 PBS. PulG surface pili were detected using an anti-PulG antibody (1:1000) and a secondary
625 anti-rabbit IgG coupled to Alexa Fluor 488 (1:200); bacteria were stained with 4',6-
626 diamidino-2-phenylindole (DAPI). Samples were observed with an inverted Leica DMRIBe
627 fluorescence microscope, and images were acquired with a Cool-Snap HQ CCD camera
628 (Roper's Instruments). Pili number and length were quantified semi-automatically using the
629 Metamorph software 6.1 (Universal Imaging) after having applied a shape filter to the images
630 to omit round-shaped unspecific dots, which were present in all samples including the
631 negative controls; the bacteria were counted manually using the same software. The non-
632 specific labelling was not taken into consideration for the quantification. Note that since
633 >95% of the fields in the *ΔpulM* and *ΔpulM* + *pulG* mutants did not have any pili, we defined
634 a relevant field of vision as a field containing at least one pilus, and only relevant fields were
635 taken into account for the quantification. The statistical significance of the differences was
636 assessed by a Kruskal-Wallis test followed by a *post-hoc* analysis using the Dunn's multiple

637 comparison tests. Graphs corresponding to pili number and length generated were built using
638 KaleidaGraph 4.1.
639
640 *Molecular dynamics simulations*
641
642 A full-length model of PulG was derived from the X-ray crystal structure of the *K.*
643 *oxytoca* PulG periplasmic domain (PDB ID: 1T92), as described in [33]. The missing 20
644 carboxy-terminal residues were modelled on the basis of close homology to GspG from
645 EHEC, and the TMS was modelled from PilA of *Pseudomonas aeruginosa* [33]. All residue
646 mutations were performed using PyMOL (The PyMOL Molecular Graphics System, Version
647 1.8 Schrödinger, LLC). The final $PulG^{WT}$ structure was composed of 133 amino acids and
648 included one calcium cation; all ionisable groups were assigned to their most probable
649 charged states at neutral pH.
650 PulG variants were then embedded in a pre-equilibrated palmitoyl-oleoyl
651 phosphatidylethanolamine (POPE) membrane, using the GROMACS g_membed tool [61]. PulG
652 position along the z-axis was guided by the presence of non-polar and hydrophobic residues
653 in the lower section of the α-helix, and interfacial aromatic residue Trp94. The systems were
654 solvated with TIP3P water, via superimposition of a pre-equilibrated box of waters, and a
655 ~0.1 M concentration of NaCl, with dimensions ~90 x 90 x 162Å. The resulting systems
656 contained ~ 36,500 water molecules and 314 lipids.
657 At each stage of system setup, steepest descent energy minimization was performed to
658 relax the protein geometry and to remove steric clashes between protein/lipid/solvent. The
659 system was equilibrated over 1.5 ns, during which position restraints, applied to all non-
660 hydrogen protein atoms, were gradually removed to relax the protein structure, membrane and
661 solvent. The Ca^{2+} ion was unrestrained during the equilibration steps yet remained in the

original bound position. Finally, 200-350 ns production MD simulations were carried out. All simulations were performed using GROMACS [62] version 4.5 [63]. The protein was treated using the CHARMM22/CMAP force field [64], and POPE lipid molecules using the CHARMM36 parameter set [64]. The parameters for MeF1 were formulated based on existing parameterized fragments. Equations of motion were integrated using the leapfrog method with a 2 fs time step, and the LINCS algorithm was used to constrain bond lengths [65]. Electrostatic interactions were computed using the Particle-Mesh-Ewald (PME) algorithm [66] and the real-space sum was cut off at 12Å. Van der Waals interactions were switched off between 10Å and 12Å. The neighbour list was updated every 10 steps. Simulations were performed using conditions of constant temperature (310 K) and pressure (1 atm) via the Bussi thermostat [67], and semi-isotropic pressure-coupling using the Parrinello-Rahman barostat [68] with a coupling constant of 5 ps, under periodic-boundary conditions. Visual analyses and preparation of molecular graphics from the simulation trajectories were performed using VMD [69]. Further analysis was performed using GROMACS and graphs were prepared with Grace (http://plasma-gate.weizmann.ac.il/Grace/). Simulations were performed using the Darwin Supercomputer of the University of Cambridge High Performance Computing Service.

Acknowledgements

We thank Evelyne Richet and Jenny-Lee Thomassin for insightful comments and critical reading of the manuscript. We thank Cesar Valencia and Jenny-Lee Thomassin for help with IF data processing and statistical analysis, Mariette Bonnet for help and advice, and Stéphane Romero for stimulating discussions about biological fibres. We are grateful to all members of the Laboratory of Intercellular Communication and Microbial Infections and of the Laboratory for Macromolecular Systems and Signalling for helpful discussions and

687 friendly support. We thank Gouzel Karimova and Daniel Ladant for the strains, plasmids and
688 advice concerning the BAC2H analysis. This work was funded by the ANR FiberSpace grant
689 N°ANR-14-CE09-0004. Javier Santos-Moreno was funded by a fellowship from the Basque
690 Government; Alexandra East was supported by an EPSRC PhD studentship. The
691 computational work benefited from use of the Darwin Supercomputer of the University of
692 Cambridge High Performance Computing Service (http://www.hpc.cam.ac.uk/), provided by
693 Dell Inc. using Strategic Research, Infrastructure Funding from the Higher Education Funding
694 Council for England. The authors state that they have no conflict of interest.

695
696 **References**

697 1. Berry, J. L. & Pelicic, V. (2015). Exceptionally widespread nanomachines
698 composed of type IV pilins: the prokaryotic Swiss Army knives. *FEMS Microbiology*
699 *Reviews* 39, 134-54.

700 2. Jarrell, K. F. & Albers, S. V. (2012). The archaellum: an old motility structure with
701 a new name. *Trends in Microbiology* 20, 307-12.

702 3. Makarova, K. S., Koonin, E. V. & Albers, S. V. (2016). Diversity and Evolution of
703 Type IV pili Systems in Archaea. *Front Microbiol* 7, 667.

704 4. Pohlschroder, M. & Esquivel, R. N. (2015). Archaeal type IV pili and their
705 involvement in biofilm formation. *Front Microbiol* 6, 190.

706 5. Melville, S. & Craig, L. (2013). Type IV pili in Gram-positive bacteria. *Microbiology*
707 *and Molecular Biology Reviews* 77, 323-41.

708 6. Korotkov, K. V., Sandkvist, M. & Hol, W. G. (2012). The type II secretion system:
709 biogenesis, molecular architecture and mechanism. *Nat Rev Microbiol* 10, 336-51.

710 7. Campos, M., Cisneros, D. A., Nivaskumar, M. & Francetic, O. (2013). The type II
711 secretion system - a dynamic fiber assembly nanomachine. *Res Microbiol* 164, 545-55.

712 8. Nivaskumar, M. & Francetic, O. (2014). Type II secretion system: A magic
713 beanstalk or a protein escalator. *Biochim Biophys Acta*.

714 9. Strom, M. S. & Lory, S. (1991). Amino acid substitutions in pilin of Pseudomonas
715 aeruginosa. Effect on leader peptide cleavage, amino-terminal methylation, and pilus
716 assembly. *J Biol Chem* 266, 1656-64.

717 10. Strom, M. S., Nunn, D. N. & Lory, S. (1993). A single bifunctional enzyme, PilD,
718 catalyzes cleavage and N-methylation of proteins belonging to the type IV pilin family.

719 *Proceedings of the National Academy of Sciences of the United States of America* 90, 2404-
720 8.

721 11. Strom, M. S., Bergman, P. & Lory, S. (1993). Identification of active-site cysteines
722 in the conserved domain of PilD, the bifunctional type IV pilin leader peptidase/N-
723 methyltransferase of Pseudomonas aeruginosa. *Journal of Biological Chemistry* 268,
724 15788-94.

725 12. Chang, Y. W., Rettberg, L. A., Treuner-Lange, A., Iwasa, J., Sogaard-Andersen, L. &
726 Jensen, G. J. (2016). Architecture of the type IVa pilus machine. *Science* 351, aad2001.

727 13. Possot, O., d'Enfert, C., Reyss, I. & Pugsley, A. P. (1992). Pullulanase secretion in
728 Escherichia coli K-12 requires a cytoplasmic protein and a putative polytopic
729 cytoplasmic membrane protein. *Molecular Microbiology* 6, 95-105.

730 14. Py, B., Loiseau, L. & Barras, F. (2001). An inner membrane platform in the type II
731 secretion machinery of Gram-negative bacteria. *EMBO Rep* 2, 244-8.

732 15. Chami, M., Guilvout, I., Gregorini, M., Remigy, H. W., Muller, S. A., Valerio, M., Engel,
733 A., Pugsley, A. P. & Bayan, N. (2005). Structural insights into the secretin PulD and its
734 trypsin-resistant core. *Journal of Biological Chemistry* 280, 37732-41.

735 16. Sauvonnet, N., Vignon, G., Pugsley, A. P. & Gounon, P. (2000). Pilus formation and
736 protein secretion by the same machinery in Escherichia coli. *EMBO Journal* 19, 2221-8.

737 17. Durand, E., Bernadac, A., Ball, G., Lazdunski, A., Sturgis, J. N. & Filloux, A. (2003).
738 Type II protein secretion in Pseudomonas aeruginosa: the pseudopilus is a multifibrillar
739 and adhesive structure. *Journal of Bacteriology* 185, 2749-58.

740 18. Gray, M. D., Bagdasarian, M., Hol, W. G. & Sandkvist, M. (2011). In vivo cross-
741 linking of EpsG to EpsL suggests a role for EpsL as an ATPase-pseudopilin coupling
742 protein in the Type II secretion system of Vibrio cholerae. *Mol Microbiol* 79, 786-98.

743 19. Sandkvist, M., Hough, L. P., Bagdasarian, M. M. & Bagdasarian, M. (1999). Direct
744 interaction of the EpsL and EpsM proteins of the general secretion apparatus in Vibrio
745 cholerae. *Journal of Bacteriology* 181, 3129-35.

746 20. Abendroth, J., Murphy, P., Sandkvist, M., Bagdasarian, M. & Hol, W. G. (2005). The
747 X-ray structure of the type II secretion system complex formed by the N-terminal
748 domain of EpsE and the cytoplasmic domain of EpsL of Vibrio cholerae. *J Mol Biol* 348,
749 845-55.

750 21. Camberg, J. L., Johnson, T. L., Patrick, M., Abendroth, J., Hol, W. G. & Sandkvist, M.
751 (2007). Synergistic stimulation of EpsE ATP hydrolysis by EpsL and acidic
752 phospholipids. *EMBO J* 26, 19-27.

753 22. Michel, G., Bleves, S., Ball, G., Lazdunski, A. & Filloux, A. (1998). Mutual
754 stabilization of the XcpZ and XcpY components of the secretory apparatus in
755 Pseudomonas aeruginosa. *Microbiology* 144 (Pt 12), 3379-86.

23. Johnson, T. L., Scott, M. E. & Sandkvist, M. (2007). Mapping critical interactive sites within the periplasmic domain of the Vibrio cholerae type II secretion protein EpsM. *Journal of Bacteriology* 189, 9082-9.

24. Possot, O. M., Vignon, G., Bomchil, N., Ebel, F. & Pugsley, A. P. (2000). Multiple interactions between pullulanase secreton components involved in stabilization and cytoplasmic membrane association of PulE. *J Bacteriol* 182, 2142-52.

25. Nivaskumar, M., Santos-Moreno, J., Malosse, C., Nadeau, N., Chamot-Rooke, J., Tran Van Nhieu, G. & Francetic, O. (2016). Pseudopilin residue E5 is essential for recruitment by the type 2 secretion system assembly platform. *Molecular Microbiology* 101, 924-41.

26. Georgiadou, M., Castagnini, M., Karimova, G., Ladant, D. & Pelicic, V. (2012). Large-scale study of the interactions between proteins involved in type IV pilus biology in Neisseria meningitidis: characterization of a subcomplex involved in pilus assembly. *Mol Microbiol* 84, 857-73.

27. Karuppiah, V., Collins, R. F., Thistlethwaite, A., Gao, Y. & Derrick, J. P. (2013). Structure and assembly of an inner membrane platform for initiation of type IV pilus biogenesis. *Proc Natl Acad Sci U S A* 110, E4638-47.

28. Tammam, S., Sampaleanu, L. M., Koo, J., Manoharan, K., Daubaras, M., Burrows, L. L. & Howell, P. L. (2013). PilMNOPQ from the Pseudomonas aeruginosa type IV pilus system form a transenvelope protein interaction network that interacts with PilA. *J Bacteriol* 195, 2126-35.

29. Pasloske, B. L., Scraba, D. G. & Paranchych, W. (1989). Assembly of mutant pilins in Pseudomonas aeruginosa: formation of pili composed of heterologous subunits. *Journal of Bacteriology* 171, 2142-7.

30. Aas, F. E., Winther-Larsen, H. C., Wolfgang, M., Frye, S., Lovold, C., Roos, N., van Putten, J. P. & Koomey, M. (2007). Substitutions in the N-terminal alpha helical spine of Neisseria gonorrhoeae pilin affect Type IV pilus assembly, dynamics and associated functions. *Molecular Microbiology* 63, 69-85.

31. Pugsley, A. P. (1993). Processing and methylation of PuIG, a pilin-like component of the general secretory pathway of Klebsiella oxytoca. *Mol Microbiol* 9, 295-308.

32. Vignon, G., Kohler, R., Larquet, E., Giroux, S., Prevost, M. C., Roux, P. & Pugsley, A. P. (2003). Type IV-like pili formed by the type II secreton: specificity, composition, bundling, polar localization, and surface presentation of peptides. *J Bacteriol* 185, 3416-28.

33. Campos, M., Nilges, M., Cisneros, D. A. & Francetic, O. (2010). Detailed structural and assembly model of the type II secretion pilus from sparse data. *Proc Natl Acad Sci U S A* 107, 13081-6.

34. Nivaskumar, M., Bouvier, G., Campos, M., Nadeau, N., Yu, X., Egelman, E. H., Nilges, M. & Francetic, O. (2014). Distinct docking and stabilization steps of the pseudopilus conformational transition path suggest rotational assembly of type IV pilus-like fibers. *Structure* 22, 685-96.

35. Cisneros, D. A., Bond, P. J., Pugsley, A. P., Campos, M. & Francetic, O. (2012). Minor pseudopilin self-assembly primes type II secretion pseudopilus elongation. *EMBO J* 31, 1041-53.

36. Karimova, G., Pidoux, J., Ullmann, A. & Ladant, D. (1998). A bacterial two-hybrid system based on a reconstituted signal transduction pathway. *Proc Natl Acad Sci U S A* 95, 5752-6.

37. Dautin, N., Karimova, G., Ullmann, A. & Ladant, D. (2000). Sensitive genetic screen for protease activity based on a cyclic AMP signaling cascade in Escherichia coli. *Journal of Bacteriology* 182, 7060-6.

38. Durand, E., Michel, G., Voulhoux, R., Kurner, J., Bernadac, A. & Filloux, A. (2005). XcpX controls biogenesis of the Pseudomonas aeruginosa XcpT-containing pseudopilus. *J Biol Chem* 280, 31378-89.

39. Lybarger, S. R., Johnson, T. L., Gray, M. D., Sikora, A. E. & Sandkvist, M. (2009). Docking and assembly of the type II secretion complex of Vibrio cholerae. *Journal of Bacteriology* 191, 3149-61.

40. Buddelmeijer, N., Krehenbrink, M., Pecorari, F. & Pugsley, A. P. (2009). Type II secretion system secretin PulD localizes in clusters in the Escherichia coli outer membrane. *Journal of Bacteriology* 191, 161-8.

41. Kolappan, S., Coureuil, M., Yu, X., Nassif, X., Egelman, E. H. & Craig, L. (2016). Structure of the Neisseria meningitidis Type IV pilus. *Nat Commun* 7, 13015.

42. Craig, L., Volkmann, N., Arvai, A. S., Pique, M. E., Yeager, M., Egelman, E. H. & Tainer, J. A. (2006). Type IV pilus structure by cryo-electron microscopy and crystallography: implications for pilus assembly and functions. *Mol Cell* 23, 651-62.

43. Craig, L., Taylor, R. K., Pique, M. E., Adair, B. D., Arvai, A. S., Singh, M., Lloyd, S. J., Shin, D. S., Getzoff, E. D., Yeager, M., Forest, K. T. & Tainer, J. A. (2003). Type IV pilin structure and assembly: X-ray and EM analyses of Vibrio cholerae toxin-coregulated pilus and Pseudomonas aeruginosa PAK pilin. *Molecular Cell* 11, 1139-50.

44. Lemkul, J. A. & Bevan, D. R. (2011). Characterization of interactions between PilA from Pseudomonas aeruginosa strain K and a model membrane. *J Phys Chem B* 115, 8004-8.

45. Andersson, H. & von Heijne, G. (1994). Membrane protein topology: effects of delta mu H+ on the translocation of charged residues explain the 'positive inside' rule. *EMBO Journal* 13, 2267-72.

46. Pasloske, B. L. & Paranchych, W. (1988). The expression of mutant pilins in Pseudomonas aeruginosa: fifth position glutamate affects pilin methylation. *Mol Microbiol* 2, 489-95.

47. Thomas, N. A., Bardy, S. L. & Jarrell, K. F. (2001). The archaeal flagellum: a different kind of prokaryotic motility structure. *FEMS Microbiology Reviews* 25, 147-74.

834 48. Albers, S. V. & Meyer, B. H. (2011). The archaeal cell envelope. *Nat Rev Microbiol*
835 9, 414-26.

836 49. Ota, A., Gmajner, D., Sentjurc, M. & Ulrih, N. P. (2012). Effect of growth medium pH
837 of Aeropyrum pernix on structural properties and fluidity of archaeosomes. *Archaea*
838 2012, 285152.

839 50. Trincone, A., Nicolaus, B., Palmieri, G., De Rosa, M., Huber, R., Huber, G., Stetter, K.
840 O. & Gambacorta, A. (1992). Distribution of complex and core lipids within new
841 hyperthermophilic members of the *Archaea* domain. *Systematic and Applied*
842 *Microbiology* 15, 11-17.

843 51. Lallemand, M., Login, F. H., Guschinskaya, N., Pineau, C., Effantin, G., Robert, X. &
844 Shevchik, V. E. (2013). Dynamic interplay between the periplasmic and transmembrane
845 domains of GspL and GspM in the type II secretion system. *PLoS One* 8, e79562.

846 52. Leighton, T. L., Dayalani, N., Sampaleanu, L. M., Howell, P. L. & Burrows, L. L.
847 (2015). Novel Role for PilNO in Type IV Pilus Retraction Revealed by Alignment
848 Subcomplex Mutations. *Journal of Bacteriology* 197, 2229-38.

849 53. Pardee, A. B., Jacob, F. & Monod, J. (1959). The genetic control and cytoplaslic
850 expression of "inducibility" in the synthesis of β-galactosidase by *E. coli*. *J Mol Biol* 1,
851 165-178.

852 54. Pugsley, A. P., Bayan, N. & Sauvonnet, N. (2001). Disulfide bond formation in
853 secreton component PulK provides a possible explanation for the role of DsbA in
854 pullulanase secretion. *Journal of Bacteriology* 183, 1312-9.

855 55. Kohler, R., Schafer, K., Muller, S., Vignon, G., Diederichs, K., Philippsen, A., Ringler,
856 P., Pugsley, A. P., Engel, A. & Welte, W. (2004). Structure and assembly of the pseudopilin
857 PulG. *Mol Microbiol* 54, 647-64.

858 56. Bartolome, B., Jubete, Y., Martinez, E. & de la Cruz, F. (1991). Construction and
859 properties of a family of pACYC184-derived cloning vectors compatible with pBR322
860 and its derivatives. *Gene* 102, 75-8.

861 57. Spratt, B. G., Hedge, P. J., te Heesen, S., Edelman, A. & Broome-Smith, J. K. (1986).
862 Kanamycin-resistant vectors that are analogues of plasmids pUC8, pUC9, pEMBL8 and
863 pEMBL9. *Gene* 41, 337-42.

864 58. Schagger, H. & von Jagow, G. (1987). Tricine-sodium dodecyl sulfate-
865 polyacrylamide gel electrophoresis for the separation of proteins in the range from 1 to
866 100 kDa. *Analytical Biochemistry* 166, 368-79.

867 59. Abràmoff, M. D., Magalhães, P. J. & Ram, S. J. (2004). Image processing with
868 ImageJ. *Biophoton Int* 11, 36-43.

869 60. Miller, J. H. (1972). *Experiments in molecular genetics*, Cold Spring Harbor
870 Laboratory, Cold Spring Harbor, New York.

61. Wolf, M. G., Hoefling, M., Aponte-Santamaria, C., Grubmuller, H. & Groenhof, G. (2010). g_membed: Efficient insertion of a membrane protein into an equilibrated lipid bilayer with minimal perturbation. *J Comput Chem* 31, 2169-74.

62. Hess, B., Kutzner, C., van der Spoel, D. & Lindahl, E. (2008). GROMACS 4: Algorithms for Highly Efficient, Load-Balanced, and Scalable Molecular Simulation. *J Chem Theory Comput* 4, 435-47.

63. Bjelkmar, P., Larsson, P., Cuendet, M. A., Hess, B. & Lindahl, E. (2010). Implementation of the CHARMM Force Field in GROMACS: Analysis of Protein Stability Effects from Correction Maps, Virtual Interaction Sites, and Water Models. *J Chem Theory Comput* 6, 459-66.

64. MacKerell, A. D., Bashford, D., Bellott, M., Dunbrack, R. L., Evanseck, J. D., Field, M. J., Fischer, S., Gao, J., Guo, H., Ha, S., Joseph-McCarthy, D., Kuchnir, L., Kuczera, K., Lau, F. T., Mattos, C., Michnick, S., Ngo, T., Nguyen, D. T., Prodhom, B., Reiher, W. E., Roux, B., Schlenkrich, M., Smith, J. C., Stote, R., Straub, J., Watanabe, M., Wiorkiewicz-Kuczera, J., Yin, D. & Karplus, M. (1998). All-atom empirical potential for molecular modeling and dynamics studies of proteins. *J Phys Chem B* 102, 3586-616.

65. Hess, B. (1997). Periodic patterns in biochemical reactions. *Quarterly Reviews of Biophysics* 30, 121-76.

66. Essmann, U., Perera, L., Berkowitz, M. L., Darden, T., Lee, H. & Pedersen, L. G. (1995). A smooth particle mesh Ewald potential. *Journal of Chemical Physics* 103, 8577–8592.

67. Bussi, G., Donadio, D. & Parrinello, M. (2007). Canonical sampling through velocity rescaling. *Journal of Chemical Physics* 126, 014101.

68. Parrinello, M. & Rahman, A. (1981). Polymorphic transitions in single crystals: A new molecular dynamics method. *J Appl Phys* 52, 7182-7190.

69. Humphrey, W., Dalke, A. & Schulten, K. (1996). VMD: visual molecular dynamics. *Journal of Molecular Graphics* 14, 33-8, 27-8.

70. Waterhouse, A. M., Procter, J. B., Martin, D. M., Clamp, M. & Barton, G. J. (2009). Jalview Version 2-a multiple sequence alignment editor and analysis workbench. *Bioinformatics* 25, 1189-91.

Figures

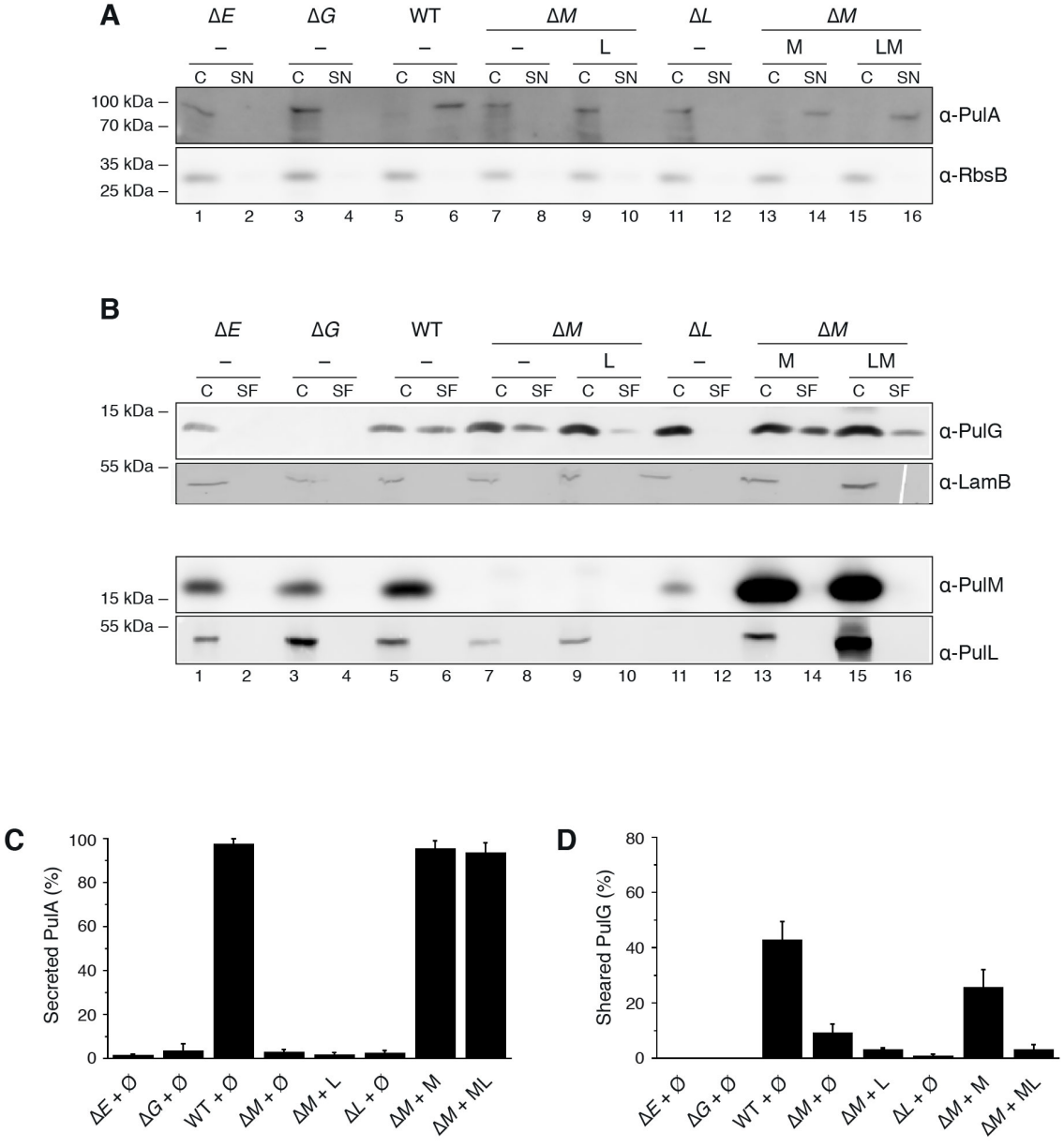

Fig. 1. The role of PulM in T2SS function

A. PulA secretion assay in near-chromosomal expression conditions using *E. coli* PAP5299 co-transformed with pCHAP8185 (all *pul* genes, WT) or its derivatives containing single nonpolar *pul* gene deletions as indicated by a single letter code: *ΔE* (pCHAP8200), *ΔG* (pCHAP8184), *ΔM* (pCHAP8496), or *ΔL* (pCHAP8251); and with compatible pSU19 (-) or its derivatives carrying indicated *pul* genes: L (pCHAP8258), M (pCHAP1353) or LM (pCHAP8843). The amount of pullulanase PulA in 0.015 OD_{600} units of cell extracts (C) and

culture supernatants (SN) was assessed by Western blot. Immunodetection of the periplasmic ribose-binding protein RbsB in 0.03 OD_{600} units served as a lysis control. Molecular weight (Mw) markers and lane numbers are shown.

B. PulG pilus assembly assay of *E. coli* PAP7460 overexpressing the *pul* genes from the same plasmids as in (A). Cell (C) and sheared pili (SF) fractions from an equivalent of 0.05 OD_{600} units were separated on Tris-Tricin SDS-PAGE, transferred onto nitrocellulose membranes and probed with antibodies against PulG, LamB, PulM and PulL. Mw markers and lane numbers are shown.

C. Quantification of the percentage of secreted PulA (mean + standard deviation - s.d.) from three independent experiments as the one in (A). Ø indicates empty vector.

D. Quantification of the percentage of sheared PulG (mean + s.d.) from three independent experiments like the one in (B). Ø, empty vector.

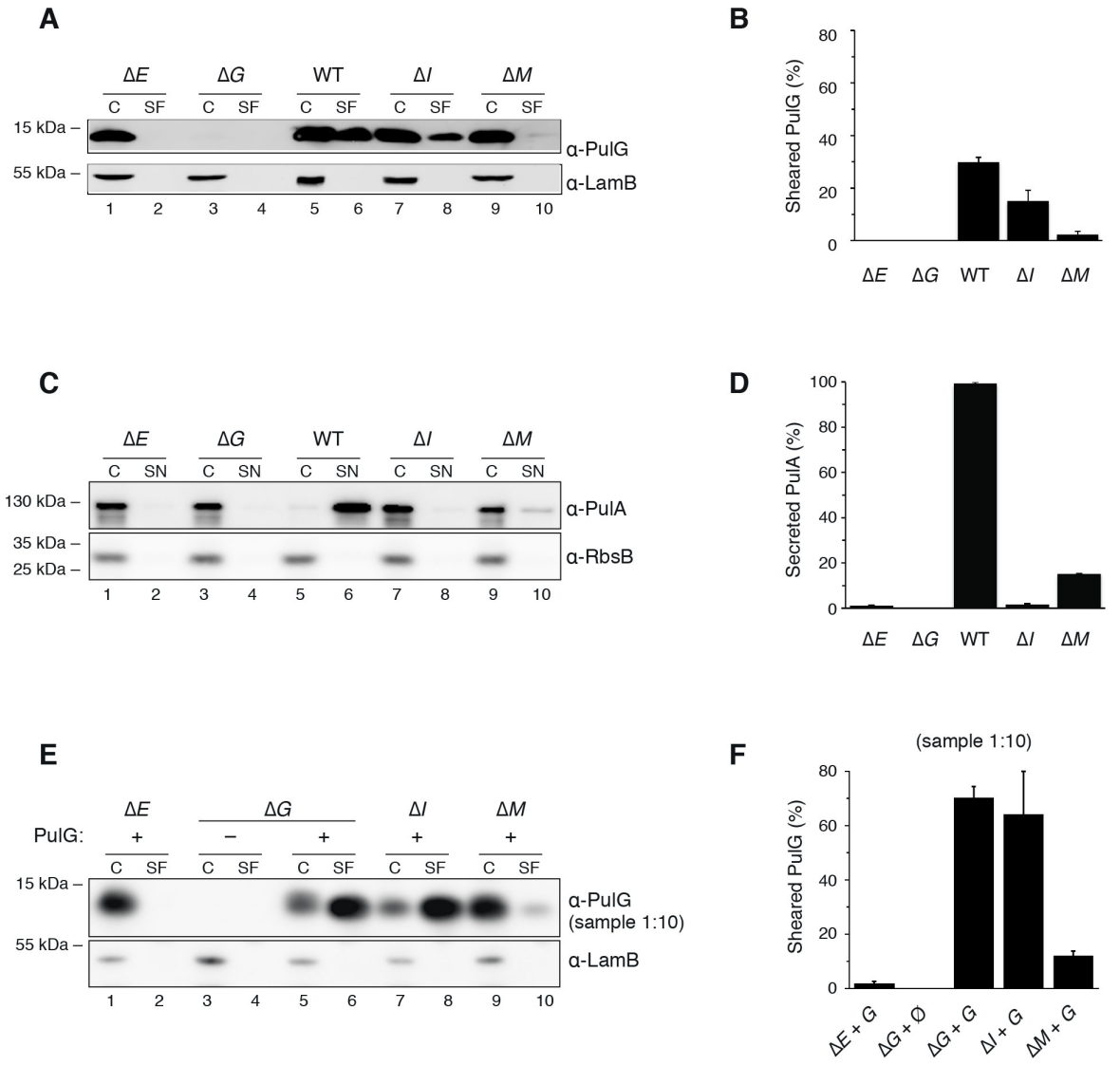

926

927 **Fig. 2. Characterisation of *ΔpulM* mutant function under conditions of *pul* gene**
928 **overexpression.**

929 Shearing (A and E) and secretion (C) assays and the corresponding quantifications of the
930 percentage of sheared PulG (mean + s.d.) (B and F) or secreted PulA (D) in three independent
931 experiments.

932 A. Immunodetection of PulG 0.05 OD_{600} units of cell (C) and sheared fractions (SF) of *E. coli*
933 PAP7460 transformed with plasmid pCHAP8185 containing all *pul* genes (WT) or its single
934 gene deletion derivatives: *ΔE* (pCHAP8200), *ΔG* (pCHAP8184), *ΔI* (pCHAP8218) and *ΔM*
935 (pCHAP8496). LamB immuno-detection is shown as control. Mw markers are indicated on
936 the left.

B. Percent of sheared PulG (mean + s.d.) from three independent experiments like the one shown in (A).

C. PulA secretion assay using transformed PAP7460 derivatives as in (A). PulA was detected by Western blot in 0.02 OD_{600} units of cell extracts (C) and culture supernatants (SN). Immunodetection of periplasmic RbsB served as a lysis control. Mw markers and lane numbers are shown.

D. Quantification of the percentage of secreted PulA (mean + s.d.) from three independent experiments like the one in (C).

E. Effect of *pulG* overexpression on pseudopilus assembly. Top: Anti-PulG immunoblot of 0.005 OD_{600} units ("sample 1:10") of cell (C) and sheared fractions (SF) of bacteria transformed with pSU19 (-) or its derivative pCHAP8658 encoding PulG (+) and indicated *pul* gene expression plasmids containing single gene deletions, as in (A): *ΔE* (pCHAP8200), *ΔG* (pCHAP8184), *ΔI* (pCHAP8218), or *ΔM* (pCHAP8496). Bottom: Anti-LamB control of a 10-fold concentrated sample (i.e. 0.05 OD_{600} units). The position of the Mw markers is indicated.

F. Percent (mean + s.d.) of PulG in the sheared fraction from three independent experiments as in (E), using 0.005 OD_{600} units ("sample 1:10"). Ø, empty vector.

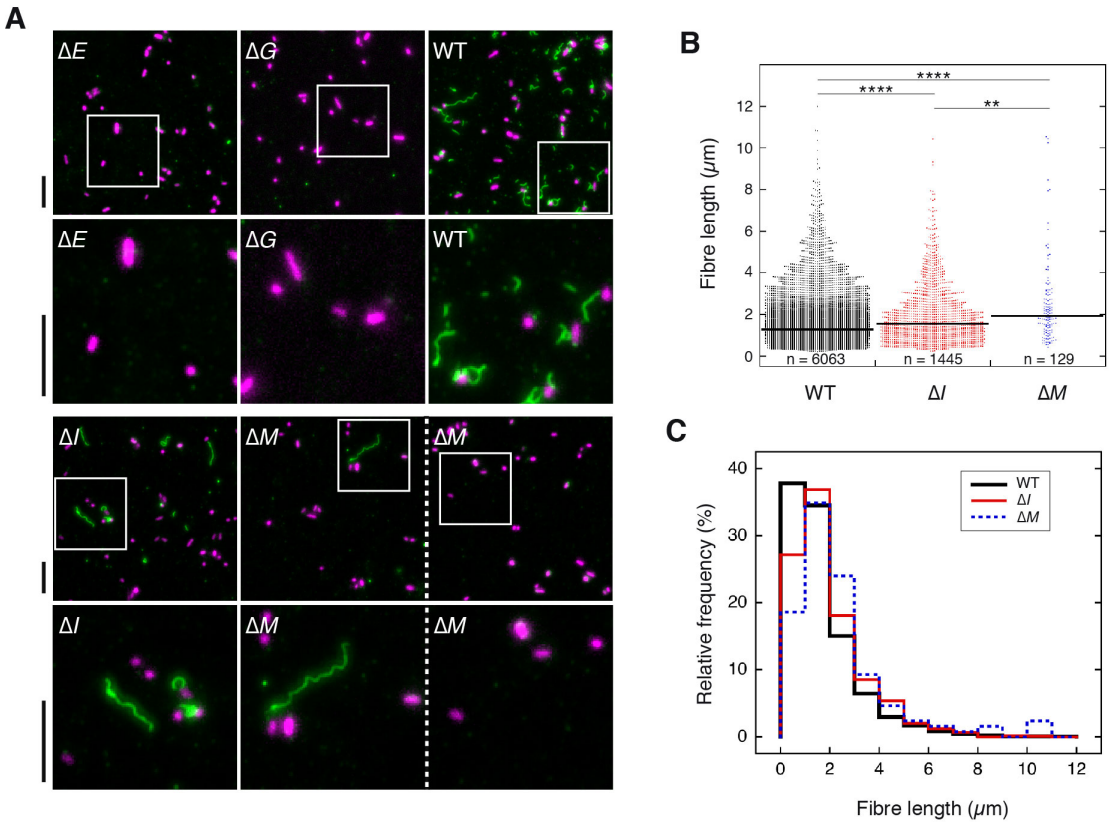

955
956 **Fig. 3. Quantitative IF microscopy analysis of piliation in *ΔpulM* mutants.**

957 Bacteria (magenta) and PulG fibres (green) were labelled and examined by IF (Materials and
958 Methods).

959 A. Representative fluorescence micrographs. WT: wild-type; *ΔE*: *ΔpulE*; *ΔG*: *ΔpulG*; *ΔI*:
960 *ΔpulI*; *ΔM*: *ΔpulM*. A 2.6-fold magnified inset is shown below each image. An additional
961 panel is shown for *ΔpulM* to illustrate the absence of fibres in the majority of the fields. Scale
962 bars = 5 µm.

963 B. Dot-plot representing the length of individual fibres (dots) scored for 12864, 13062 and
964 14786 bacteria (for WT, *ΔpulI* and *ΔpulM* respectively) in three independent experiments. On
965 average, 0.47 ± 0.09 (mean ± s.d.,) fibres per bacterium were found in WT, 0.11 ± 0.2 in
966 *ΔpulI* and 0.009 ± 0.003 in *ΔpulM* strain). The median fibre length values, shown as
967 horizontal black lines, are 1.2 ± 0.6 µm (median ± m.a.d., median absolute deviation) for WT,
968 1.5 ± 0.7 µm for *ΔpulI* strain and 1.8 ± 0.7 µm for *ΔpulM* strain. Dunn's test, **p < 0.01,
969 ****p < 0.0001.

970 C. Relative frequency distribution of fibre length. Bin size = 1 µm.

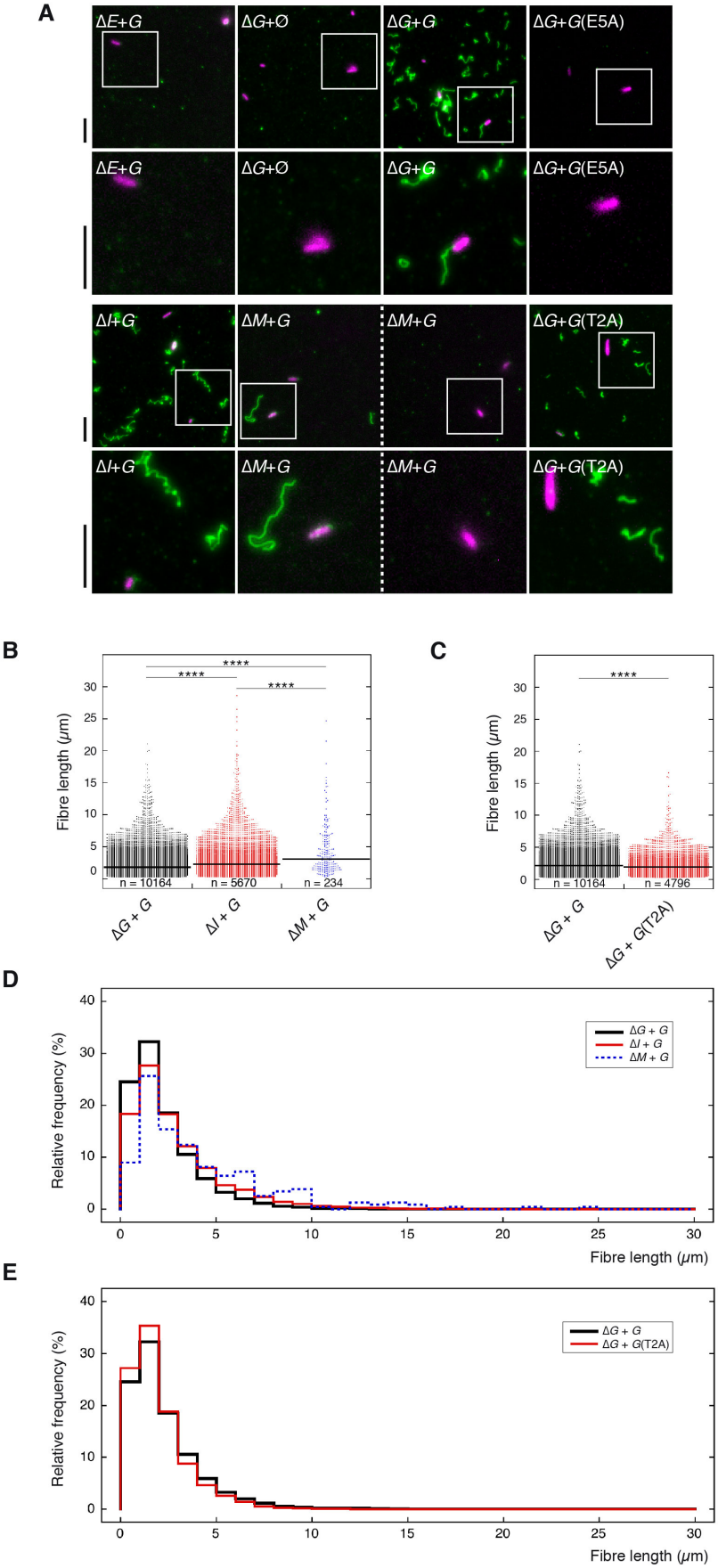
A
ΔE+G
ΔG+Ø
ΔG+G
ΔG+G(E5A)
ΔE+G
ΔG+Ø
ΔG+G
ΔG+G(E5A)
ΔI+G
ΔM+G
ΔM+G
ΔG+G(T2A)
ΔI+G
ΔM+G
ΔM+G
ΔG+G(T2A)
B
Fibre length (μm)
****
****
****
n = 10164
n = 5670
n = 234
ΔG + G
ΔI + G
ΔM + G
C
Fibre length (μm)
****
n = 10164
n = 4796
ΔG + G
ΔG + G(T2A)
D
Relative frequency (%)
ΔG + G
ΔI + G
ΔM + G
Fibre length (μm)
E
Relative frequency (%)
ΔG + G
ΔG + G(T2A)
Fibre length (μm)

Fig. 4. The effect of PulG overproduction on T2S pilus assembly.

A. IF microscopy of the piliation ability of *ΔpulM* + *pulG* and *ΔpulG* + *pulG*(T2A). Bacteria, magenta; fibres, green. A 2.6-fold magnified inset is shown below each image. An extra panel is shown for *ΔpulM* + *pulG* to illustrate the absence of fibres in most of the fields. The scale bars (5 μm) are shown on the left.

B and C. Dot-plots representing the length of individual fibres (dots) scored for 1342, 1190, 1597 and 1460 bacteria (for *ΔpulG* + *pulG*, *ΔpulI* + *pulG*, *ΔpulM* + *pulG* and *ΔpulG* + *pulG(T2A),* respectively) in three independent experiments. The number of fibres/bacterium (expressed as mean ± s.d) were 7.64 ± 1.49 (for strain *ΔpulG* + *pulG*); 4.7 ± 0.6 (for strain *ΔpulI* + *pulG*); 0.15 ± 0.06 (for strain *ΔpulM* + *pulG*); and 3.73 ± 1.68 (for strain *ΔpulG* + *pulG(T2A)*). The median values of fibre length are shown as a horizontal black lines: for *ΔpulG* + *pulG*, 1.7 ± 0.8 μm (median ± m.a.d.); for *ΔpulI* + *pulG,* 2.2 ± 1.1 μm; for *ΔpulM* + *pulG,* 3.0 ± 1.6 μm and for *ΔpulG* + *pulG(T2A),* 1.6 ± 0.7 μm. Dunn's test, ****$p < 0.0001$.

D and E. Relative frequency distributions of fibre length. Bin = 1 μm.

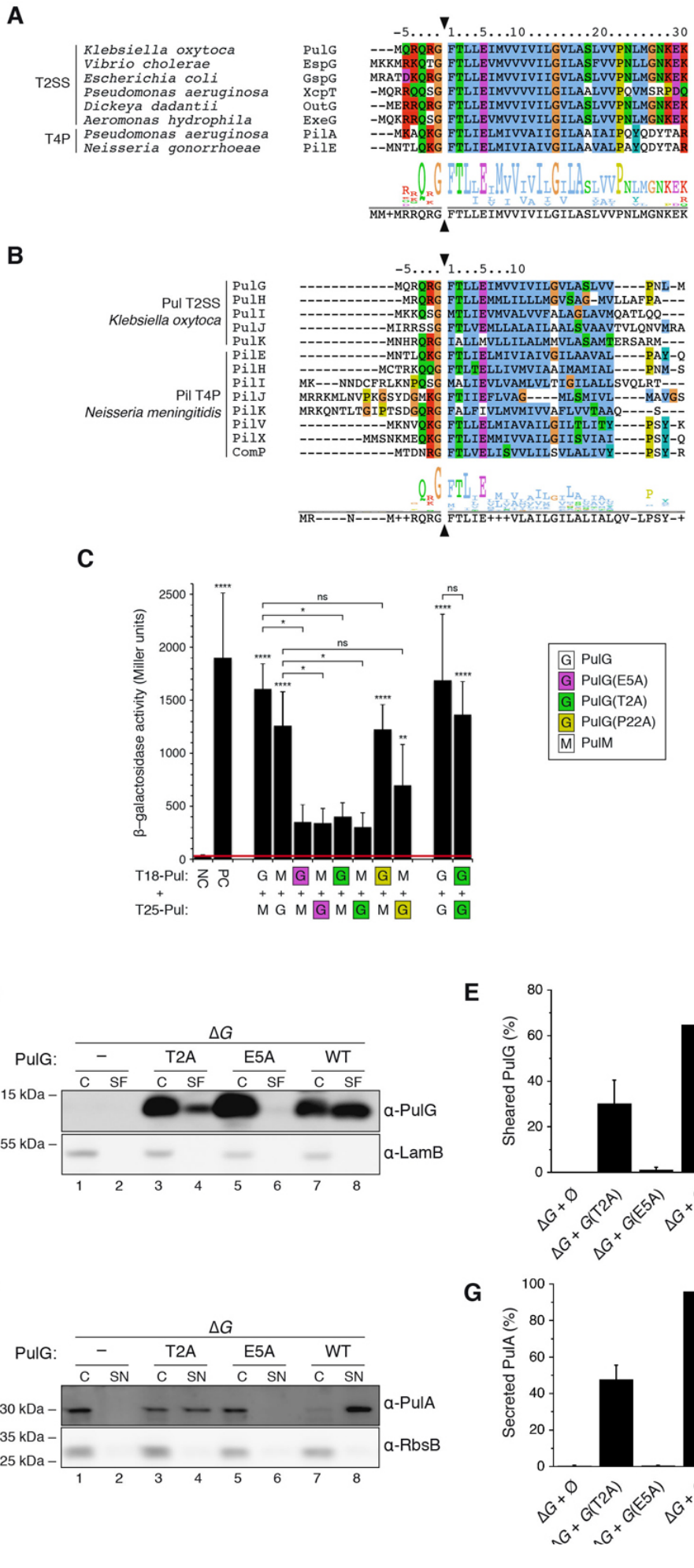
A
T2SS
T4P
Klebsiella oxytoca
Vibrio cholerae
Escherichia coli
Pseudomonas aeruginosa
Dickeya dadantii
Aeromonas hydrophila
Pseudomonas aeruginosa
Neisseria gonorrhoeae
PulG
EspG
GspG
XcpT
OutG
ExeG
PilA
PilE
MM+MRRQRG FTLLEIMVVIVILGILASLVVPNLMGNKEK
B
Pul T2SS
Klebsiella oxytoca
Pil T4P
Neisseria meningitidis
PulG
PulH
PulI
PulJ
PulK
PilE
PilH
PilI
PilJ
PilK
PilV
PilX
ComP
MR----N----M++RQRG FTLIE+++VLAILGILALIALQV-LPSY-+
C
β–galactosidase activity (Miller units)
T18-Pul:
T25-Pul:
PulG
PulG(E5A)
PulG(T2A)
PulG(P22A)
PulM
D
ΔG
PulG:
C
SF
15 kDa –
55 kDa –
α-PulG
α-LamB
E
Sheared PulG (%)
ΔG + Ø
ΔG + G(T2A)
ΔG + G(E5A)
ΔG + G
F
SN
130 kDa –
35 kDa –
25 kDa –
α-PulA
α-RbsB
G
Secreted PulA (%)

Fig. 5. PulG^{T2A} variant shows defective interaction with PulM, piliation and secretion.

A. Protein sequence alignment of the N-terminal segments of major T2SS pseudopilin and T4P subunits from the indicated bacterial species. The consensus sequence is indicated below and arrowheads indicate the prepilin peptidase cleavage site.

B. Sequence alignment of major and minor pseudopilins from the Pul T2SS of *Klebsiella oxytoca* (top) and major and minor T4P pilins from *Neisseria meningitidis* (bottom). The arrowheads indicate the prepilin peptidase cleavage site. Alignments were generated using Jalview2 software [70].

C. BAC2H analysis of the interactions between T18 and T25 hybrids with PulM and PulG and its derivatives PulG^{E5A}, PulG^{T2A} and PulG^{P22A}. β-galactosidase activity was measured in at least 6 independent colonies co-transformed with pUT18c and pKT25 plasmid derivatives (Table 1) as described in Materials and Methods. Bar graphs indicate mean values and error bars indicate standard deviation. Statistically significant values relative to the negative control are indicated above each bar. The difference between certain positive interactions was assessed for statistical significance and represented by horizontal lines indicating the compared strains. NC, activity of bacteria producing T18 and T25 as negative control; PC, activity of positive control strain producing T18-Zip and T25-Zip chimera. The red horizontal line indicates the background mean β-galactosidase activity measured in the negative control. *p < 0.05; **p < 0.01; ****p < 0.0001; ns, non-significant.

D. Shearing assay of *E. coli* PAP7460 co-transformed with plasmid pCHAP8184 containing all *pul* genes except *pulG* (*ΔG*) complemented with pSU19 (-) or its derivatives carrying *pulG* alleles: WT (pCHAP8658), T2A (pCHAP8732) or E5A (pCHAP8663). PulG immunodetection in 0.05 OD_{600} units of cell and sheared fractions (C, SF). Below, immunodetection of LamB in the same samples. Lane numbers and Mw markers are depicted.

E. Quantification of the percentage of sheared PulG (mean + s.d.) from three independent experiments like the one in (D). Ø indicates an empty vector.

F. Secretion assay using *E. coli* PAP5299 transformed with the same plasmids as in (D). Immunodetection of PulA in 0.02 OD_{600} units of cell extracts (C) and supernatants (SN) is shown. α-RbsB is used as a lysis control. Mw markers and lane numbers are shown.

G. Quantification of the percentage of secreted PulA (mean + s.d.) from three independent assays like the one in (F). Ø indicates empty vector.

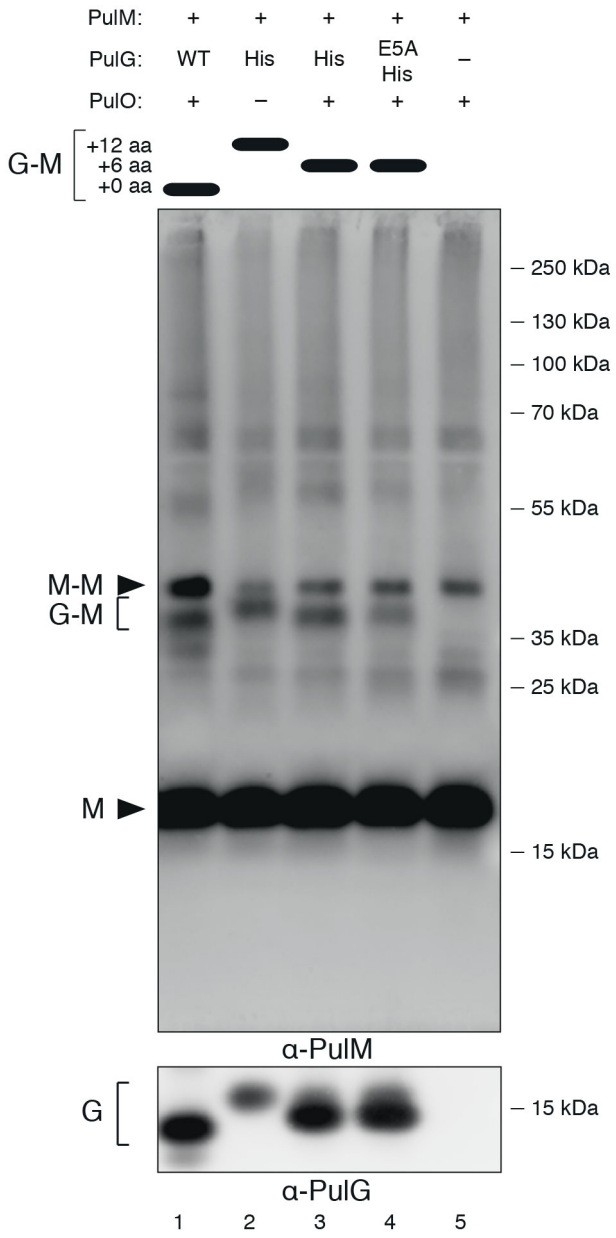

Fig. 6. PulM interacts with PulG in the context of the complete Pul T2SS.

E. coli PAP7460 carrying plasmids encoding the *pul* genes with either *ΔpulG* (pCHAP8184, lanes 1 and 3-5) or *ΔpulG* + *ΔpulNO* (pCHAP8400, lane 2) alleles were transformed with pSU19 or its derivatives encoding PulG (pCHAP8658), PulG-His_6 (pCHAP1362) or $PulG^{E5A}$-His_6 (pCHAP7785). Total extracts of strains cross-linked *in vivo* with 0.6% FA (Materials and Methods) analysed by SDS-PAGE and immunodetection with anti-PulM or anti-PulG antisera are shown. Theoretical relative migration of PulM-PulG heterodimers is depicted according to the molecular weight of the PulG variant in each case. The positions of the PulM monomers (M), PulM homodimers (M-M) and the shifting PulG-PulM heterodimers (G-M) are

indicated. For the α-PulG blot only the band corresponding to PulG monomer is shown. Mw markers and lane numbers are indicated. Uncropped images of α-PulM and α-PulG Western blots of untreated and FA-treated samples are shown in Fig. S2.

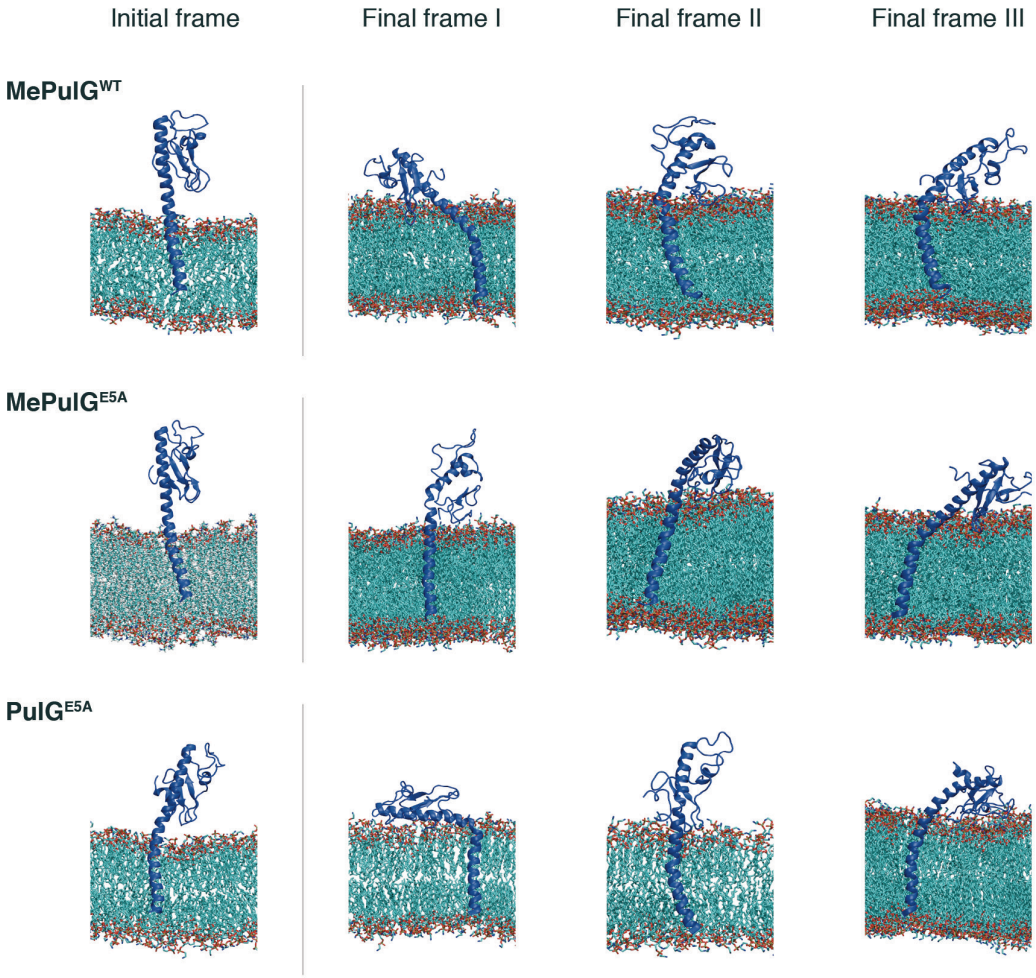

Fig. 7. Visualisation of MD simulations of PulG variants.

Snapshots of initial and representative final conformations of methylated MePulG^{WT}, methylated MePulG^{E5A}, and non-methylated PulG^{E5A} variants embedded in a POPE bilayer. In all the simulations, the protein became more deeply buried, and in all (except PulG^{E5A} replica II) the protein bent towards the membrane surface, allowing the globular domain to interact with the phospholipids. Changes in F1 and E5 did not cause severe protein destabilization or membrane perturbation.

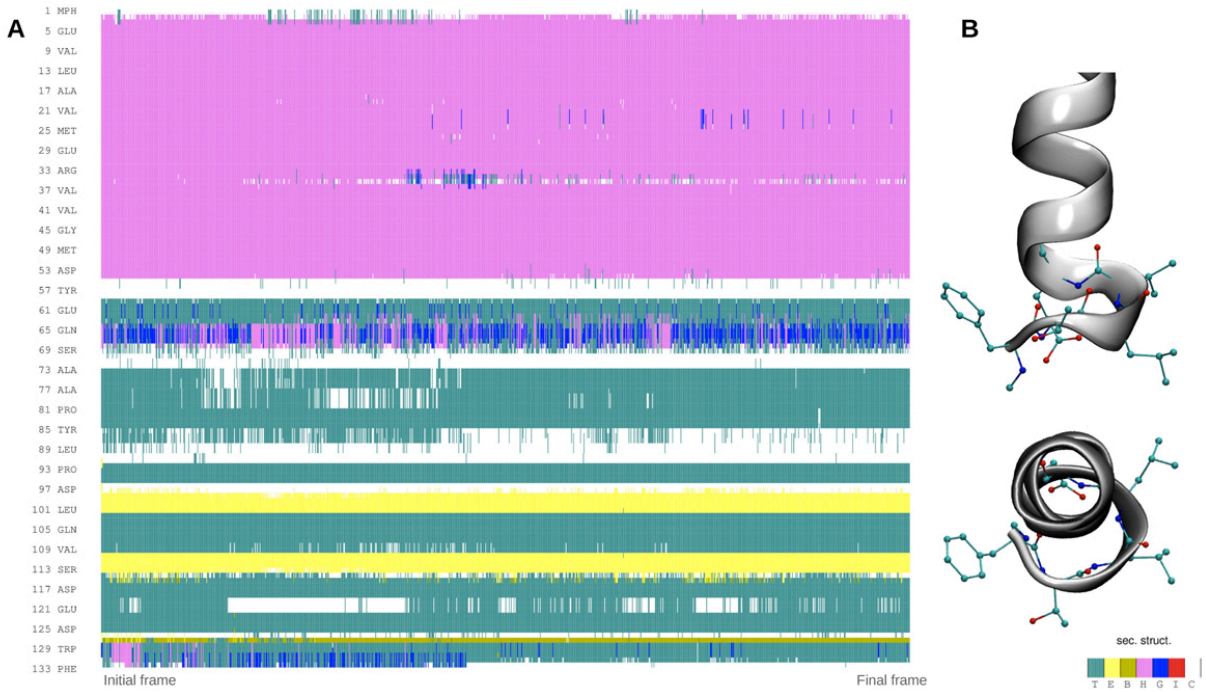

Fig. 8. Secondary structure of PulG during MD simulations.

A. A representative data set showing the maintenance of protein secondary structure during a MePulG^{WT} simulation. The graph shows the evolution of the secondary structure of each residue (y-axis) over time (x-axis), coloured as follows: α-helix – purple; 3-10 helix – blue; β-sheet – yellow; turn – cyan; coil – white. In MePulG^{WT} simulations the first several residues demonstrated a relaxation of helical structure into either turn or coil structures, suggesting that MeF1 and E5 destabilized the terminus as they deformed to interact with each other.

B. The MeF1-E5 interaction caused the N-terminus to deform and created a loop, shown here with the protein backbone in grey and residues 1-5 shown as ball-and-stick structures, coloured by atom (carbon – cyan, oxygen – red, nitrogen – blue).

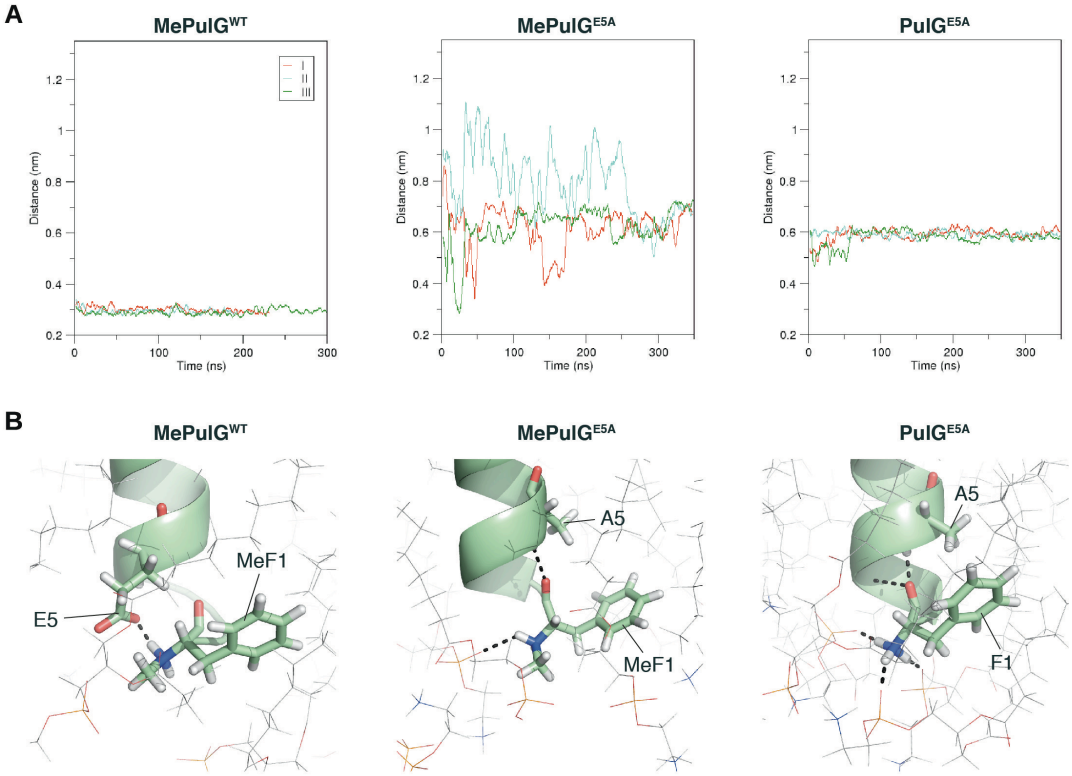

Figure 9. N-terminal intra-molecular and protein-lipid interactions.

A. Graphs showing how the minimum distances between the residue 1 methyl group or amide terminus with any atom of the residue 5 side-chain varied during the simulations. In the MePulG^{WT} system the methyl group of MeF1 and the E5 side-chain remained consistently within 3Å of each other, whereas in the mutant systems the distances were much larger. This suggested that MePulG^{WT} E5 promotes intra-molecular interactions with the N-terminal positive charge of MeF1, anchoring PulG less firmly in the bilayer and priming the protein for extraction during pseudopilus assembly. In contrast, the N-terminus of the MePulG^{E5A} and PulG^{E5A} mutant variants interact with membrane lipids, anchoring the protein.

B. Representative visualisations of hydrogen bonding of PulG N-terminus to POPE and solvent; the protein is shown as a green ribbon, with the labelled residues in stick format and coloured by atom (C – green, O – red, N – blue, H – white). Hydrogen bonds are shown as black dotted lines. POPE is depicted in stick format and coloured by atom (C – grey, O – red, N – blue, H – white, P – orange).